THE UNIVERSITY OF MICHIGAN
COLLEGE OF LITERATURE, SCIENCE, AND THE ARTS
Department of Physics

Technical Report

INVESTIGATION OF DI-PION RESONANCES IN 3.7 BeV/c π^-p COLLISIONS

Yong Yung Lee

ORA Project 04938

under contract with:

U.S. ATOMIC ENERGY COMMISSION
CHICAGO OPERATIONS OFFICE
CONTRACT NO. AT(11-1)-1112
ARGONNE, ILLINOIS

administered through:

OFFICE OF RESEARCH ADMINISTRATION ANN ARBOR

May 1964

TABLE OF CONTENTS

TABLE OF CONTENTS (Concluded)

LIST OF TABLES

LIST OF FIGURES

LIST OF FIGURES (Concluded)

CHAPTER I

INTRODUCTION

During the past few years, much attention has been given to resonances of elementary particles in high-energy physics. In fact many resonances including pion-nucleon, pion-hyperon, pion-kayon, and multipion resonances, have been found in this period.[1,2]

Several pion-nucleon resonances, called nucleon isobars, have been found with different values of mass, spin and isotopic spin as well as many multipion resonances including ρ, ω, and f. One can expect that more will be found in the future. A great deal of study has been done on these resonances, yet there are many things still to be determined about them.

In this experiment, we took 60,000 pictures in the 20-in. hydrogen bubble chamber at the Brookhaven National Laboratory. Our beam was a 3.7 BeV/c separated π^- beam from the 33 BeV Alternating Gradient Synchrotron (AGS). This report will deal with the reactions

$$\pi^- + p \rightarrow \pi^- + \pi^+ + n$$

$$\pi^- + p \rightarrow \pi^- + \pi^\circ + p \quad .$$

These can be identified by two out-going charged-particle tracks. A preliminary report on this experiment and a paper dealing with the four-prong events have been reported elsewhere.[3-5]. The complete report on the four-prong events and elastic scattering will be reported in separate

papers.

The main things one can study with the above reactions are nucleon isobars with masses up to about 2.6 BeV and dipion resonances with masses up to 1.7 BeV. Since, unfortunately, isobar formation in the reactions was very meager, very little was done with the isobars. The pion-pion resonances seen in the reactions are one centered at 765 MeV and another centered at 1250 MeV effective mass. They are ρ and f°, respectively.

The existence of the ρ was predicted by Frazer et al.,[6] and soon thereafter several experiments showed evidence for a resonance in the T = 1 state (T is the isotopic spin) with a mass value of approximately 750 MeV.[7-9] Since then, many other experimenters have studied ρ and found its quantum numbers to be of isotopic spin 1, spin 1, parity -, G-parity +. f° was first found by Selove et al.,[10] and has since been studied by several other groups.[3,11,12] Most probably its quantum numbers are isotopic spin 0, spin 2, parity +, and G-parity +. This f°-resonance might well fit into the pattern of Regge trajectories,[14,15] however, its quantum numbers are not yet definite.[16]

We studied these two resonances by employing a pion-pion scattering model which was suggested by Chew and Low[17] to analyze scattering on unstable targets. Recent experimental evidence[12,18] shows that this method serves as a good model for analyzing pion-pion resonances. The fact that the target pion is virtual, however, makes the interpretation of such scattering somewhat indefinite. Using this method an attempt was made to extrapolate the results into the nonphysical region in order to get

the real pion-pion scattering cross section.

CHAPTER II

PARTICLES, RESONANCES AND THEIR INTERACTIONS

In the previous chapter we used the terms "particles" and "resonances" many times. The detailed meaning of these words can be found in various articles. The author thought, however, it is necessary to give a brief description of what is meant by these terms, and the quantities related to them. The word "particle" means an elementary particle, which is characterized by being a subatomic particle. There are 30 elementary particles which have been known for some time. These consist of 16 baryons and antibaryons, 7 mesons, 6 leptons, and the photon. The term "baryon" refers to nucleons and to the group of particles which are heavier than the neutron called hyperons. The term "lepton" refers to another group of particles which are lighter than the π-meson and consists of muons, electrons, and massless neutrinos, along with their antiparticles. The family of "mesons" consists of the three charge states of the pions and four kinds of kayons. The kayons and hyperons are classified as strange particles. They are normally produced only in strong interactions and decay only through weak interactions.

The first so-called "resonance" was discovered in the year 1952 by Enrico Fermi and his colleagues. They found that the scattering cross section of pions on protons, measured as a function of energy, had a sharp peak for 1238 million electron volts (MeV) center-of-mass energy

in the pion-proton system. Since then several other such pion-nucleon resonance peaks have been found. These peaks were found not only in pion-proton elastic scattering but also in the effective mass of the final state pion-nucleon pairs in which several other out-going particles were produced. The effective mass of a group of particles can be calculated by the equation

$$(\text{Effective mass})^2 = (\Sigma E_i)^2 - (\Sigma \vec{P}_i)^2$$

where E_i and $\vec{P}_i$ are the total energy and the momentum vector of ith particle. It is a Lorentz-invariant quantity, which represents the total energy of the system in its center-of-momentum reference frame. In addition to the pion-nucleon resonances, many other kinds of resonances have been found, including pion-hyperon, pion-kayon, and multipion resonances.

There have been several attempts to classify this large number of resonances and particles into groups having similar properties. The currently most popular schemes are the so-called "eightfold way" and "Regge trajectory." The eightfold way predicts that particles should fall into groups having one, eight, or ten members with the same spin and parity. The Regge trajectory hypothesis predicts that a given group should reoccur as another group with spin differing by two integer units. In this scheme there is no fundamental difference between a "particle" and a "resonance." What is commonly referred to as a "particle" is simply a relatively stable (long-lived) member of the group and what is commonly

referred to as a "resonance" is simply a relatively short-lived member. For a more complete discussion of these ideas the reader is referred to a recent article in Scientific American.[25]

These particles or resonances can be characterized by their mass and various quantum numbers. We discuss below some of these quantum numbers, since frequent reference will be made to them in this thesis. We first consider the spin angular momentum of particle, denoted by J. A particle can have a spin of only an integral or half-integral multiple of Plank's constant $\hbar$, which is the fundamental constant of quantum theory. The mesons have integer J-values while nucleons have half-integer values. A second quantum number in which we will be interested is the isotopic spin T. This is not directly related to the spin angular momentum, although its mathematical behavior in quantum mechanics is very similar to that of the spin angular momentum. The idea of isotopic spin predicts that small subgroups (isotopic multiplets) of particles should have approximately equal masses and that the behavior of the individual members of a multiplet under the strong interactions should not depend on their charge. The number of members of a particle multiplet is given by $2T+1$. We will also make use of the intrinsic parity of particles which can have values ± 1 (sometimes referred to as even or odd, or simply + or -). This characterizes the behavior of the wave function of the particle under space inversion (i.e., reversal of the directions of x, y, and z). The parity is conserved in strong and electromagnetic

interactions but not in weak interactions. The meaning of the terms "strong," "electromagnetic," and "weak" interactions will be given later in this chapter. The G-parity of the particles is only applicable to states in which both baryon number and strangeness is zero. This is conserved only in strong interactions.

If there is more than one type of resonance between the same pair of particles, as in the case of the isobars, one usually gives the mass and the quantum numbers to identify them. For instance the isobar at 1238 MeV is denoted by 1238,3/2,3/2 or simply 3/2,3/2 which are its isotopic-spin and angular-momentum quantum numbers, respectively. This isobar belongs to the same Regge trajectory as the 1720 MeV isobar (angular momentum 7/2) and in the eightfold way it belongs to a decuplet.

We would like to devote the last part of this chapter to describing kinds of interactions between these particles. The strongest of these is called the "strong" interaction. The range of the force is very short (about 10^{-13} cm), however, its strength is about 10^{39} times that of the gravitational force. It is the force that holds nuclei together. The interactions involving strong forces conserve every quantum number mentioned above. The next strongest interaction is due to the familiar "electromagnetic" force which is about 100 times weaker than the strong interaction and has a much longer range. The "weak" interaction has strength of only 10^{-14} of the strong interaction, and is believed to have a very short range. The elementary particles can participate in all of these interactions.

The great differences in the strengths of these forces are responsible for the great differences observed in the lifetimes of particles. A particle which can decay through a strong interaction can be expected to have a lifetime of about 10^{-22} sec whereas if only electromagnetic decays are available, its lifetime will be several orders of magnitude longer. Weak interactions lead to lifetimes which are typically 10^{-6} to 10^{-10} sec. Particles with very short lifetimes will have experimentally detectable widths (i.e., uncertainty in their mass) given by the uncertainty principle $\Delta m \sim \hbar/\tau$, where $\hbar$ is Planck's constant (6.58×10^{-22} MeV-sec) and τ is the lifetime in seconds. An experimental observation of this effect will be seen later in our data on the ρ- and f°-resonances.

CHAPTER III

EXPERIMENTAL EQUIPMENT AND BEAM SETUP

3.1 BUBBLE CHAMBER

The particle detection apparatus used in this experiment is the Brookhaven 20 in. hydrogen bubble chamber. The shape is rectangular, 10x10x20 in., with the beam entering from the 10x10 in. side. To take pictures two windows are placed on both 20x10 in. sides and a mercury arc is placed some distance behind the rear window. Four cameras are placed in front of the chamber with their optic axes perpendicular to the window and the intersections of these axes with the front window forms a 9 in. sq. During each expansion of the chamber the four cameras take a picture of the chamber when the arc flashes. The time between the expansion and the arc flash employed in this experiment is around 140 μsec in order to produce the optimum bubble size. The magnetic field inside the chamber is perpendicular to the windows and its spatial and time variation is negligible.

There are 11 fiducial marks on the windows, four on the front window and seven on the rear window. The position of the fiducial marks is known to be better than 0.01 cm with respect to the optic axes of the cameras. A more detailed description of the chamber can be found elsewhere.[19,20]

3.2 BEAM SETUP

The 3.7 BeV/c π^--beam used in this experiment was obtained from Brookhaven Alternating Gradient Synchrotron. The energy of the internal proton beam of the accelerator was 33 BeV and the intensity was on the order of 10^{11} protons per pulse. Only a small fraction of this was spilled onto our target, the remainder being used for another experiment. A 3-sec repetition rate was normally used. Since this experiment was parasitic, these parameters were varied because of the primary user's requirements.

The beam was designed and set up by Brookhaven personnel, and details of the design and operating conditions are given in BNL internal reports.[21,22] A brief description of the beam as it was used for this experiment, however, will be given below. The separated beam consisted of four sections: beam transport section, two separation stages, and a beam shaping section. The total beam length was 270 ft. Figure 1 shows the beam layout at the AGS building while Figure 2 shows a schematic diagram for the beam layout. Our momentum of 3.7 BeV/c is the maximum accommodated by the magnets.

The target used to produce the pions is of aluminum 0.1 in. high, 0.25 in. wide and 2 in. long in the direction of circulation of the internal proton beam. The Rapid Beam Deflector (RBD) is fired causing a small part of the circulation protons to move into the target. Since this experiment was parasitic, the RBD is fired early in the acceleration cycle in order to save most of the beam for the primary user. The

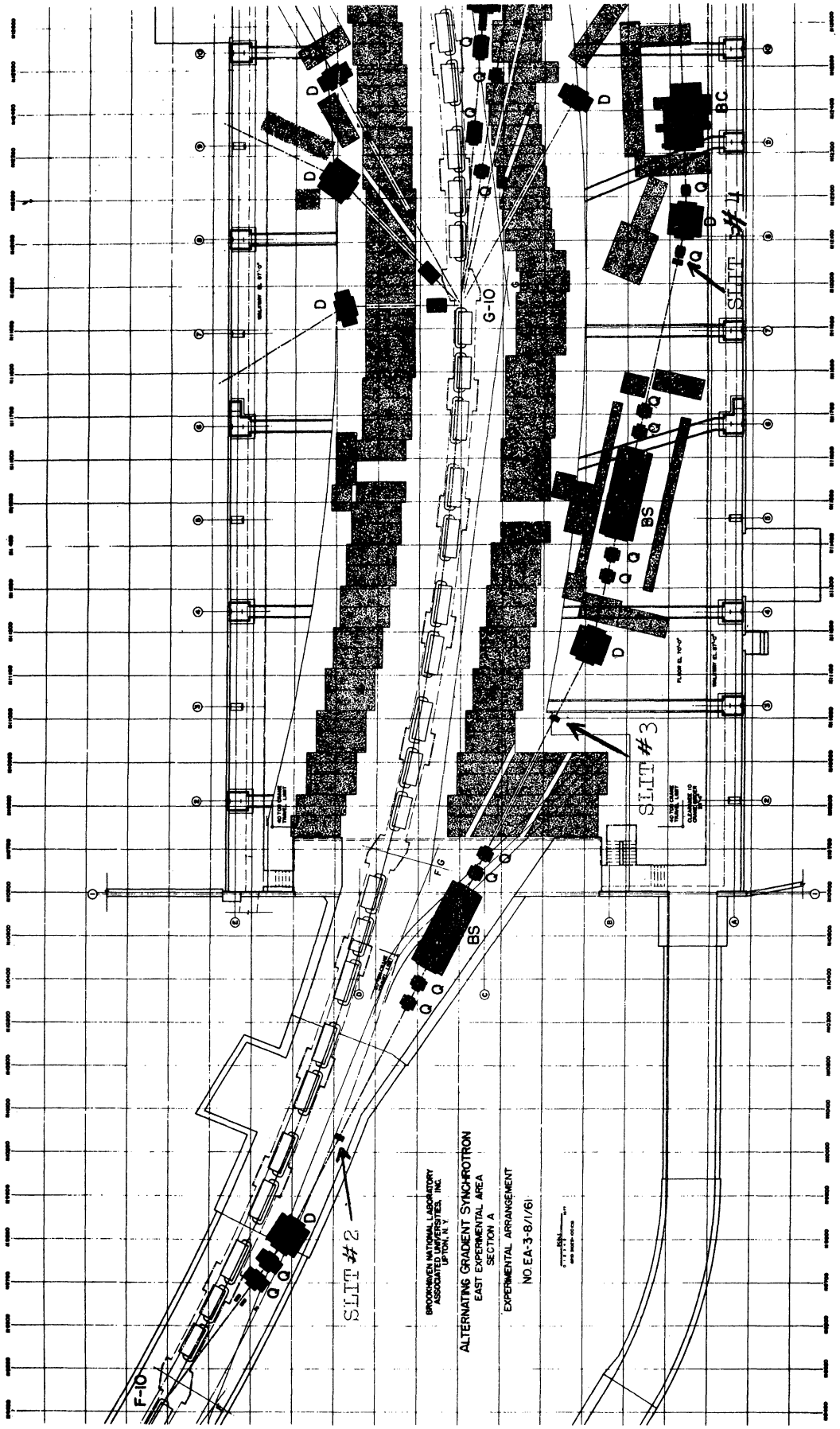

Figure 1. Beam layout at the AGS building.

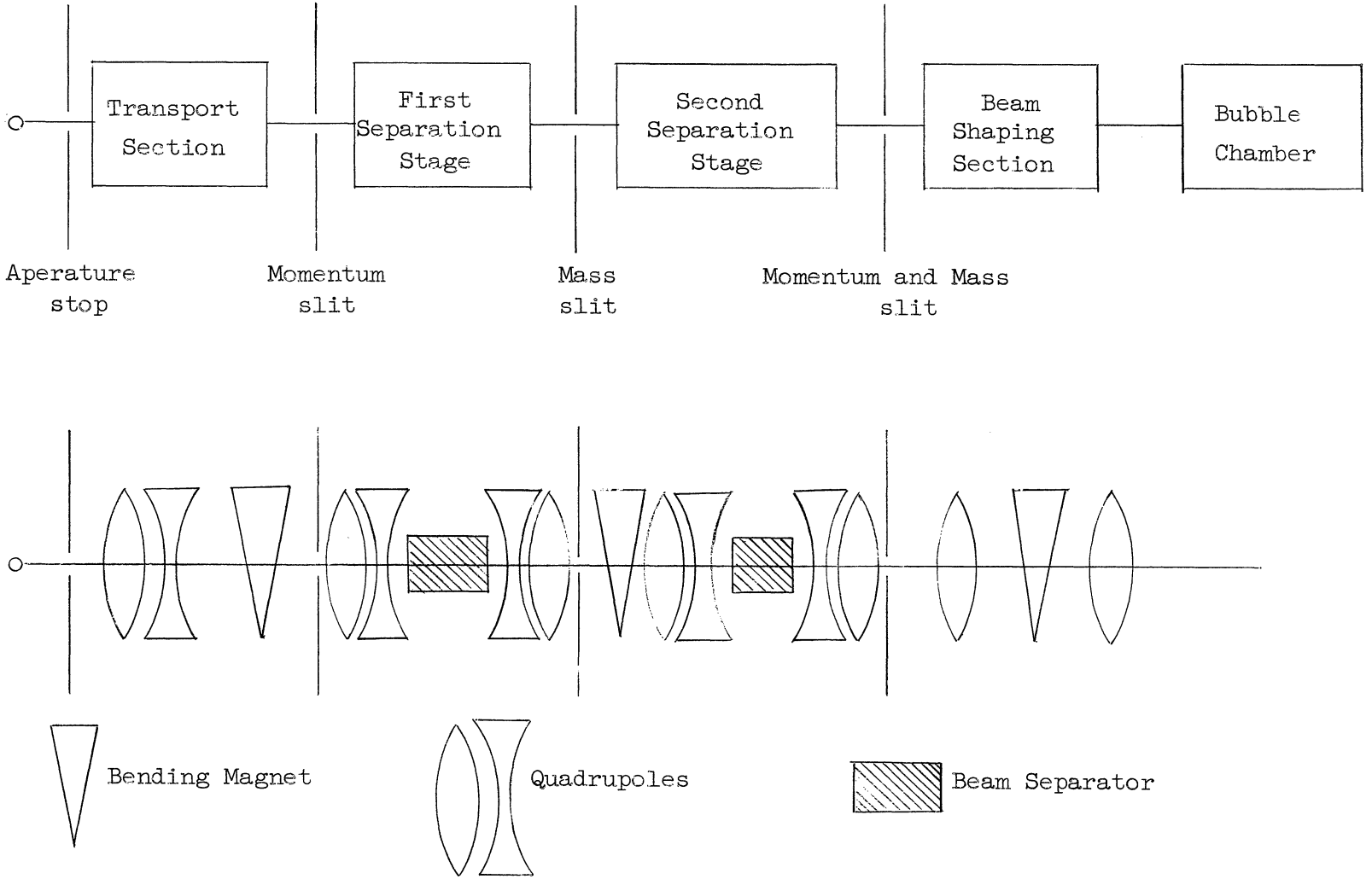

Figure 2. Schematic diagram for beam layout.

secondary beam axis in the transport section made an angle of 8° with respect to the circulating beam in order to avoid the effect of the synchrotron magnetic field. Slit 1 limits the angular acceptance of the beam to 40×10^{-6} sr, and the bending magnet in this section gives rough momentum selection. Two beam separators consisting of crossed electric and magnetic fields serve as velocity spectrometers to separate out the desired particles.[21] A bending magnet in the second beam separating stage serves as a momentum spectrometer in the same manner as the first bending magnet. The purpose of the beam shaping section is to modify the particle trajectories so that the incident beam is made of an appropriate size to fill the beam window of the bubble chamber. Twelve quadrupoles were used to focus the beam trajectories: two in the transport section, four for each beam separation stage, and two for beam shaping. Four slits separate the various sections. The dimensions of these slits are given in the table below.

TABLE I

THE DIMENSIONS OF SLITS USED FOR THE BEAM

Slit	Horizontal, in.	Vertical, in.
1	8.0	0.5
2	0.3	0.045
3	0.3	0.2
4	0.3	0.2

Beam tuning was done after setting all bending magnets and quad-

rupoles. The magnetic field in separator 1 was then varied by steps, and at each step separator 2 was varied until the π^- intensity was optimized.

According to the experiments of Cocconi et al.,[23] and Baker et al.,[24] at an angle of 8° and momentum of 3.7 BeV/c the composition of the negative beam is mainly pions with a few percent of K^- and p^-. After the two stages of beam separation there was negligible amount of K^-, p^-, and μ^-. The small remaining contamination of μ^- etc., could not give a significant effect as we normalize our cross sections to the known total cross section of π^- on protons.

During the running of this experiment, the magnetic fields of the bending magnets were checked occasionally to be sure that the beam momentum had not drifted, and the corrector coil current was frequently changed to maintain constant number of particles that entered the chamber. This corrector coil is located just behind the bending magnet in the transport section and produces a horizontal magnetic field. This field deflects the beam vertically so as to adjust the intensity that passes slit 2. The actual beam momentum, as opposed to the nominal one that the currents in the magnets were set for, has been estimated by checking the χ distribution of fitted beam momentum for the events fitted with four constraints and is 3.63 ± .02 BeV/c.

3.3 SCANNING MACHINES

The films from the 20 in. bubble chamber were cut into 100-ft strips and scanned at Randall Laboratory. The scanning machines project the

image on a green translucent screen. The size of the image is slightly larger than the actual size of the chamber. The machines have electronic view changers and film-driving devices. They can also project two views at once and have a device which moves one image relative to the other so that one view can be superimposed on another. This is useful if one wants to see if a track has stopped inside the chamber.

3.4 MEASURING DEVICE

Pictures to be measured are projected onto the same kind of screen as the scanning machine. These machines have both a low and a high magnification in order to give both an overall view of the picture and a detailed view of a small section. The lower magnification gives almost life size of the bubble chamber while the higher magnification gives about 2.8 times life size. All measuring is performed at the higher magnification.

The machine has a moving stage controlled by selsyns on which the film holders are attached. The film is held down by a vacuum in order to insure flatness. By moving the stage the measurer can position a particular point onto a fixed cross-hair attached to the screen. In this way one eliminates the nonuniformity of projection optics which can affect the accuracy of the measurement. That is to say, the coordinates of points on the film are measured directly from the motion of the film itself rather than from coordinates on the projected image.

Two kinds of digitizing methods were employed in this experiment to

measure film motion. The method used for most of the experiment was that of Moire fringe counting. A brief description of the machine is as follows. Optical heads consisting of four photodiodes and two gratings are attached to both axes of the measuring stage. The longer grating is attached to the moving part and the shorter grating and the photodiodes are on the fixed part of the stages. The two gratings are tilted relative to each other so that the grating lines make dark and light lines parallel to the measuring stage. As the stage moves the shadow of the two gratings move periodically, with one cycle corresponding to .0001-in. of stage displacement. A photodiode picks up these signal and counts the number of cycles. The advantages of this device are that one does not have to worry about backlash of the screw which moves the stage and there is no worry of a poor contact or a broken blade such as can arise in a mechanical encoder system. The third measuring machine, used for a small fraction of our analysis, makes use of a mechanical encoding device. This consists of a rotating series of contacts which produces different combinations of electrical signals for different positions of the rotator. The linear motion of the stage is coupled to the rotator motion by means of a highly accurate screw. The accuracy of all these machines is known to be better than a few microns on the film.

The film coordinates, as indicated by readings on the digitizers, were punched automatically on IBM cards which serve as input to the geometry reconstruction programs.

CHAPTER IV

DATA REDUCTION

4.1 SCANNING OF THE EVENTS

Two views of the 20-in. bubble chamber picture were used for scanning the events, since not all four views were necessary to get the needed information. On scanning the film, we made restrictions on the volume of the bubble chamber scanned, and the number of beam tracks entering this "fiducial volume." Since we needed a certain length of primary and secondary tracks to maintain measurement accuracy, we rejected the events which happened outside of the fiducial volume. This fiducial volume was taken such that the incoming beam tracks were not less than 4.5 cm in length and such that a minimum of 15 cm of forward-outgoing tracks occurred for two-prong events. Whenever more than 25 beam tracks entered the bottom of the fiducial volume the frame was ignored in order to maintain high scanning efficiency.

Scanning sheets were prepared for this particular experiment on which were noted such things as the number of nondecaying outgoing tracks (which we shall call prongs), decaying prongs, and the number of electron-positron pairs and "V particles" pointing to the interaction vertex. Electron-positron pairs and V's could be easily identified by the curvature and bubble density of the tracks. Scanners also noted whether the tracks were stopped inside of the chamber or not, and other relevant information such as the frame number, event number if there were more than

one event in the picture, roll number, identification number of the scanner, and the date

Every picture was scanned twice by different scanners independently. A physicist then checked every disagreement of the two scanners and also checked the number of tracks in any frame in which 20 to 30 tracks were listed by the scanner in order to make the 25 track cut-off accurate. Estimated scanning efficiency of this experiment was better than 95% for the nonstrange particle events in which we are interested.

4.2 MEASUREMENT

The two Moire fringe-type measuring machines were employed to measure most of the events except for those few which were measured on the mechanical encoder machine. The two best stereoscopic views were chosen in order to get the best result in the geometric reconstruction of the track. The two best views vary from track to track and are those which have the biggest angle between the projection of intersection of the line between the two cameras on the front window and the projection of the tracks on the window. As described in the previous chapter, these devices punch out the coordinates of the three to ten points on each track, two fiducial marks (permanent marks on the front glass), and other relevant information such as the sign of the charge of the particle, whether or not this track stopped inside the chamber, view number, track number, frame number, etc.

A remeasurement was done for those events which failed in either

the geometry or the kinematic programs. Typical rejected events were those which had more than two bad point measurements or had the stereoscopic angle (described above) less than 15° for any one track. This report contains all the events which did not fail by the third remeasurement.

If there is no slippage in the encoder system, the coordinates of some point should be the same both at the beginning and at the end of a measurement. It was necessary to check this for the fringe-type machines at the end of each measurement. For the mechanical encoder system, at the beginning of each day, the scanners checked to see if there was any backlash of the screw by comparing the coordinate of one point when approaching from both directions. The accuracy of these machines was about 3.5μ for the fringe system and about 5μ for the encoder system when combined with the setting error of the measurer, as described in the previous chapter.

4.3 SPATIAL RECONSTRUCTION AND KINEMATICS

After measurement, the IBM cards containing all needed information for events went through an IBM 7090 program so that possible errors in punched data could be detected and repunched in a different format to match the input of the geometry program.[26] At this stage, there were quite a few mistakes in the punching, and these were corrected before getting into the geometry program.

The geometry program used here was written in the Fortran and Fap

languages at Brookhaven National Laboratory. This program (named TRED) calculates the initial momentum and azimuthal angle of the track in a projection plane parallel to the front window of the bubble chamber, and the dip angle with respect to this projection plane. The program then makes small corrections to these quantities taking into account the loss of energy of the particle along its path. Since the range-energy relation depends on the mass of the particle, TRED gives all this geometry information for five different particles, namely electron, pion, kayon, proton, and sigma. TRED also computes the errors associated with each quantity of each track due to the experimental lack of smoothness and theoretical effect of multiple scattering. All these quantities are written on a tape which serves as the input to the kinematic program. The only quantity which was not calculated by TRED was the beam momentum, since we knew this accurately from the beam magnet setting.

The kinematic program (KICK) to analyze this experiment was originally written in Berkeley[27,28] and has been modified at Brookhaven. This program examines each vertex point (beam-interaction point) according to a set of hypotheses. On every vertex point there are four constraint equations corresponding to overall conservation of the three components of momentum and also conservation of energy:

$$\sum E_i = 0 \quad \text{and} \quad \sum \vec{P}_i = 0$$

where $\vec{P}_i$ and E_i are the momentum vector and the total energy of a particle at the vertex. We take a negative sign for an outgoing particle.

For two-charged-prong events KICK tests three reactions:

$$\pi^- + p \rightarrow \pi^- + p \qquad (1)$$

$$\rightarrow \pi^- + p + \pi^\circ \qquad (2)$$

$$\rightarrow \pi^- + \pi^+ + n \qquad (3)$$

KICK first calculates the missing momentum, energy, and mass according to the equations

$$\Delta E = \sum E_i$$

$$\Delta P = \sum \vec{P}_i$$

$$(\text{Missing Mass})^2 = (\Delta E)^2 - (\Delta P)^2$$

corresponding to each mass assignment for the charged particles. Since we were not looking for strange particles or leptons, the missing neutrals it could try were only the π° and neutron. KICK did not try to fit events containing more than one neutral because there are too many missing parameters for such hypotheses. If any one of the above three reactions seemed reasonable, KICK made a "fit" which is the process of readjusting the measured parameters in accordance with their errors so that the four conservation laws are satisfied within some allowed limit. Using the method of least squares[28,29] in the process of fitting, one can use all four constraint equations for the nonneutral case but only one constraint equation for the case of one missing neutral, since the three other equations must be used to calculate unmeasured parameters. KICK

also calculated the readjusted errors, which are smaller than the original errors. Usually the readjusted errors associated with a four constraint fit were smaller than those associated with a one constraint fit.

The goodness of fit is estimated by the χ^2 value.[29] The χ^2 probability distribution should follow the curve

$$P(\chi^2) = \frac{\exp\left(-\frac{\chi^2}{2}\right)(\chi^2)^{\left(\frac{n}{2}-1\right)}}{2^{n/2}\Gamma\left(\frac{n}{2}\right)}$$

provided that there is no systematic error, where n is number of constraints. Figure 3 shows the χ^2 distributions for events identified as reactions (2) and (3). These are consistent with theoretical curve (dashed curve). Hypotheses having a χ^2 probability of more than 2% are considered as giving a good fit and printed out in KICK output sheets. The χ^2 probability is defined as

$$\chi^2 \text{ probability} = \int_{\chi^2}^{\infty} dP(\chi^2) \quad .$$

KICK also printed out the two-particle invariant masses for every successful fit and punched out one card identifying the event and the hypothesis. Another important thing done by KICK was to calculate the theoretical ionization relative to the beam track, and to give its projected value on a plane parallel to the front window for every successful fit.

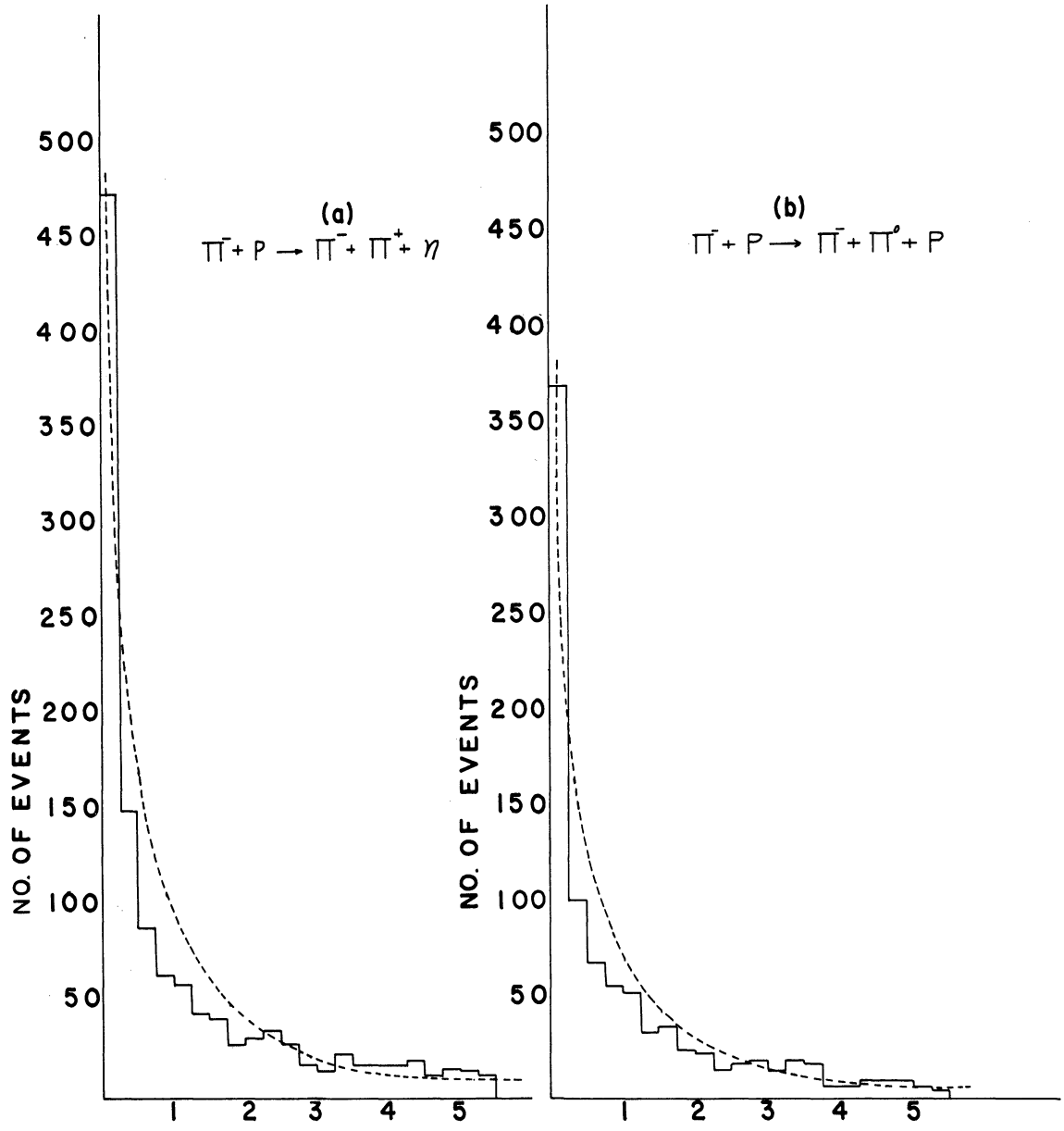

Figure 3. χ^2 distribution for unambiguous events.

4.4 EVENT IDENTIFICATION

Through the fit procedure of KICK, events often fit more than one hypothesis, as we consider that a fit means a χ^2 probability of more than 2%. To decide the correct hypothesis, physicists checked the bubble density of the tracks to see if they agreed with the bubble density predicted by KICK. Bubble density is defined as the number of bubbles per unit length of track normalized to a minimum ionizing track. As a minimum ionizing track we took a beam track, i.e., 3.7 BeV/c π^- beam. The bubble density of the track is approximately proportional to the inverse square of β, the ratio of speed of particle to the speed of light.[13] The quantity β depends on the momentum and mass of the particle according to

$$\beta = \frac{P}{\sqrt{M^2+P^2}} \quad .$$

Since we were not interested in strange-particle interactions, the negative track was always considered as π^- whereas for a positive particle choice is π^+ or proton. Therefore for negative particles we checked to see if the bubble density agreed with the π^- prediction, and for positive tracks we checked to see if the density agreed with either the π^+ or p predictions. The bubble density appearing in KICK output was actually the linear bubble density divided by the cosine of dip angle, since one can only see the track projected on the plane parallel to the front window of the bubble chamber. From our experience we could distinguish a proton from a π^+ for those cases in which the predicted bubble density

differed by at least 30 to 40%. Figure 4 shows the relation between linear bubble density and momentum. Thus, from the appearance of the track we were able to distinguish a π^+ from a proton up to around 1700 MeV/c momentum. Also, sometimes the kinematics allow only one reaction so that this case was automatically decided, unless there was an obvious bubble density disagreement. This stage still leaves a few events which are ambiguous between the different reactions. The statistics for event identification are shown below (all numbers indicate the percentage of total events). On the basis of bubble density check, the events which had a single fit for reaction (1) were never rejected. The events fitting to reactions (1) and (2) or (1), (2), and (3) were never resolved except reaction (3) was often rejected.

Further study has been made of events which remained ambiguous after this stage. Since reaction (1) is a four-constraint fit and the others are one-constraint fits the events which were ambiguous between (1) and either of the others were thrown into reaction (1). The reason for this is clear from Table II where we see that practically all of the events that fit (1) and (3) were determined to be (1) on the basis of bubble density. There were, however, ambiguous events between the two one-constraint fits. These events were considered as reaction (3) for the following reasons. First, if we look at the χ^2 distributions for these events considered as (3) (Figure 5a), and also considered as (2) (Figure 5b), we can see a definite difference between them. Even for these events which have $\chi^2 < 1$ for reaction (2), the χ^2 distribution considered as (3)

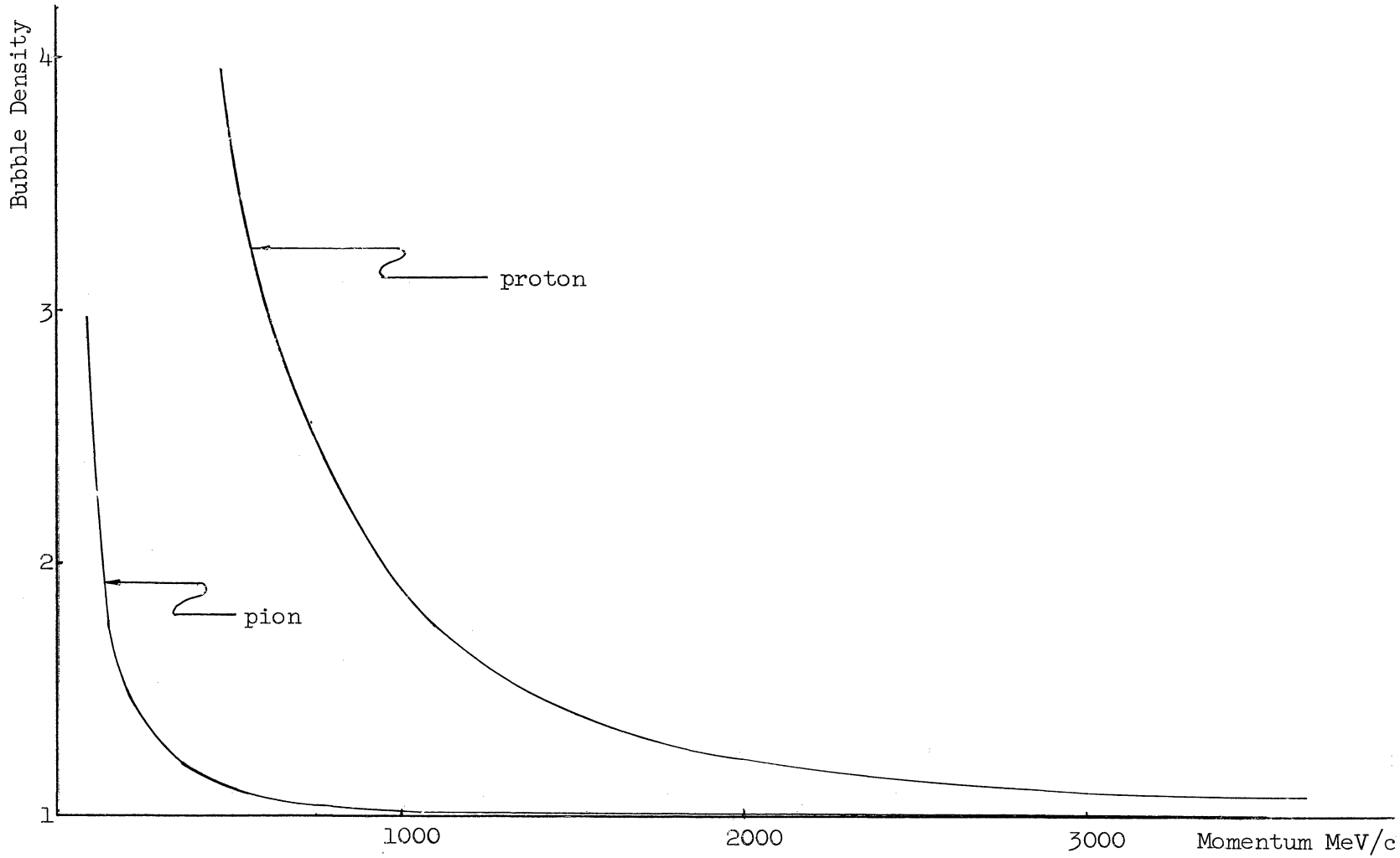

Figure 4. Relation of bubble density and particle momentum.

TABLE II

STATISTICS ON EVENT IDENTIFICATION

Percentage of Unambiguous Events (After Bubble Density Check)

Type of reaction		(1)	(2)	(3)	Rejected	Total
Single fit		4.6	8.2	13.3	6.9	33.0
Double fit	(1)&(2)	0.0	0.0	---	0.0	0.0
	(1)&(3)	20.3	---	0.1	0.0	20.4
	(2)&(3)	---	13.5	13.5	0.0	27.0
Triple fit		0.0	0.0	0.0	0.0	0.0
Total		24.9	21.7	26.8	6.9	80.4

Percentage of Remaining Ambiguous Events

Type of reaction		(1)&(2)	(1)&(3)	(2)&(3)	(1),(2)&(3)	Total
Double fit	(1)&(2)	1.2	---	---	--	1.2
	(1)&(3)	---	1.2	---	--	1.2
	(2)&(3)	---	---	6.6	--	6.6
Triple fit		10.2	0.0	0.0	.3	10.5
Total		11.4	1.2	6.6	.3	19.5

is still good (Figure 5c). Second, the momentum transfer from the incident pion to final dipion system for those ambiguous events is shown in Figure 6 and we notice reaction (3) predominates by comparing it with the distribution for good events (Figure 7). By comparing the ratio of high- and low-momentum transfer we conclude that more than 80% of these remaining ambiguous events actually belong to (3).

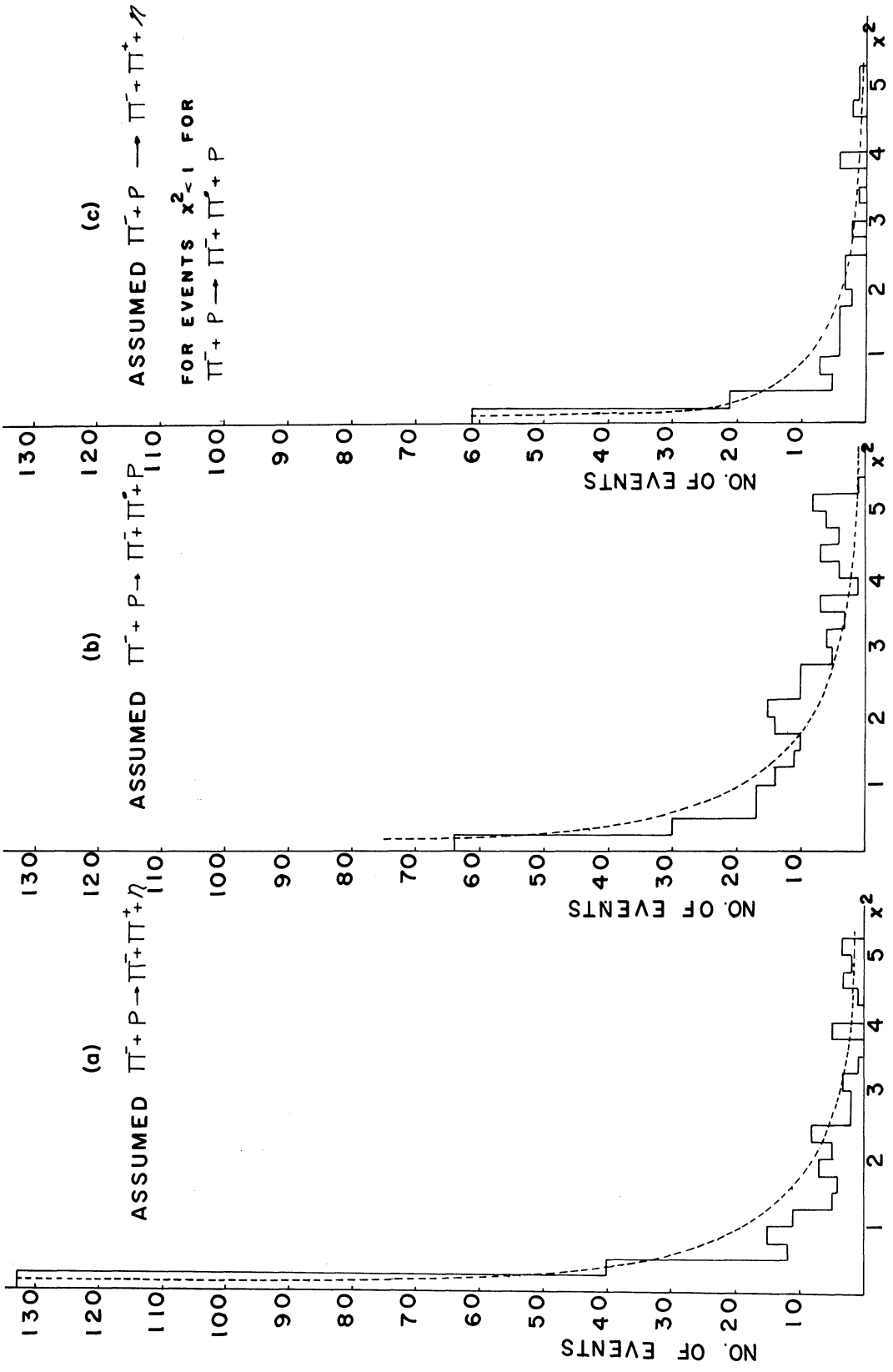

Figure 5. χ^2 distribution for ambiguous events between the two one-constraint fits.

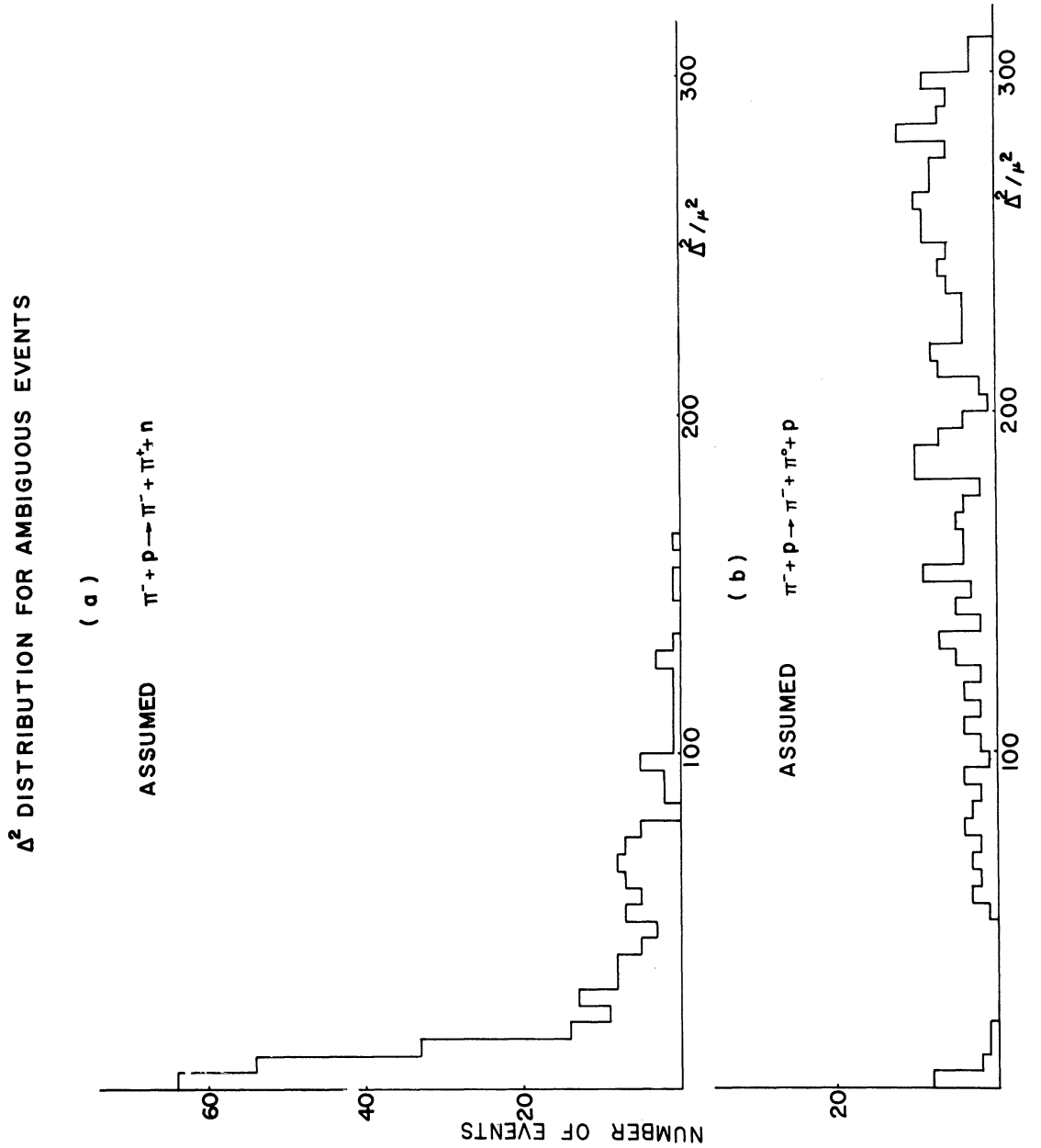

Figure 6. Δ^2 distribution for ambiguous events.

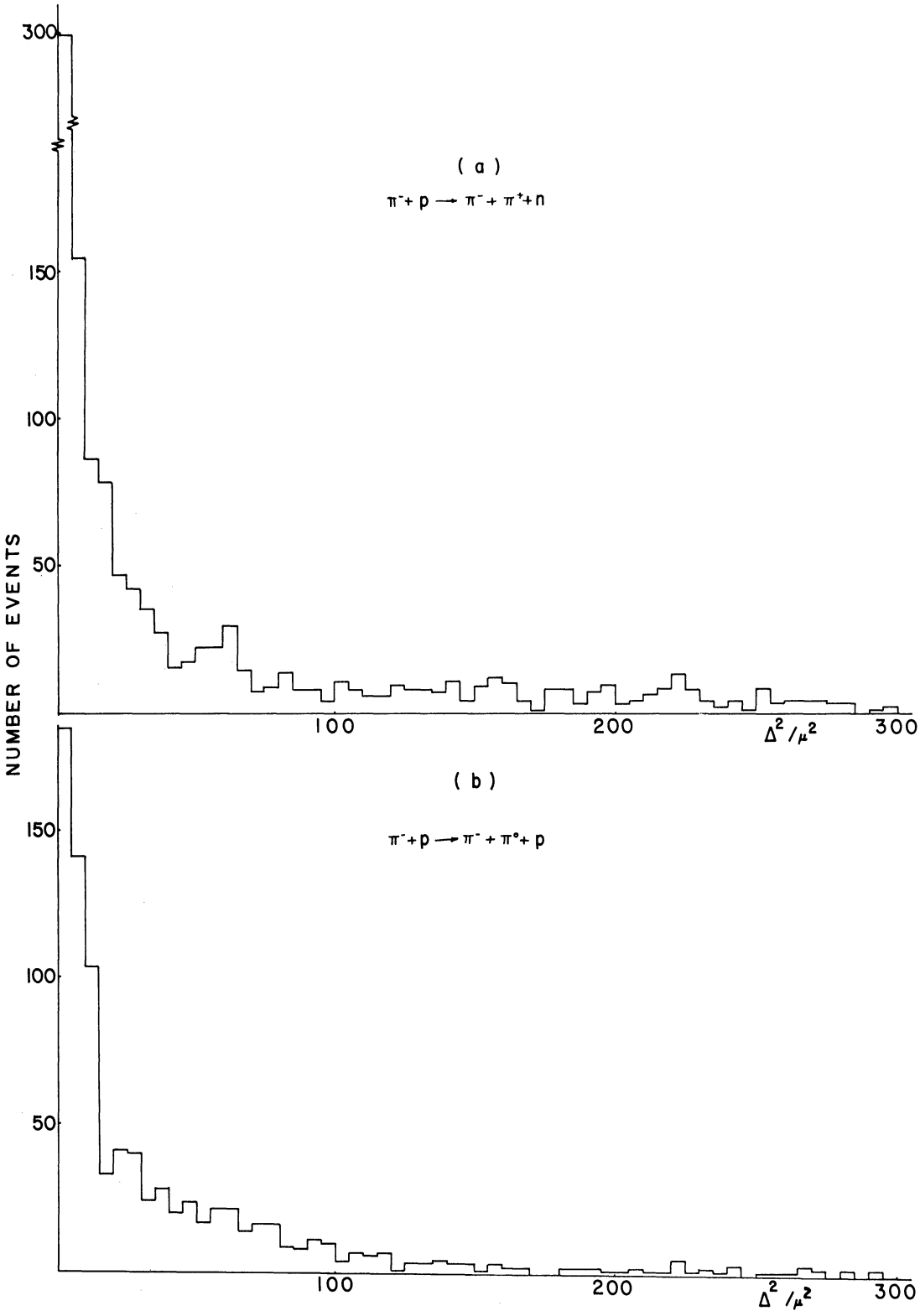

Figure 7. Δ^2 distribution for unambiguous events.

CHAPTER V

RESULTS

5.1 INTRODUCTION

In this chapter we will discuss and interpret the results of this experiment. The things which will be covered are the production and decay properties of the ρ-meson followed by a study of the f°-meson. We begin with a discussion of some of the general properties of these resonances.

5.2 GENERAL PROPERTIES OF RESONANCES

5.2.1 Distribution of Two-Particle Mass Spectrum

Figures 8 and 9 show the histograms of the various two-particle mass combinations. As explained in previous chapters all the ambiguous events between reactions (2) and (3) are included in reaction (3). The shapes of the pion-nucleon mass spectra will be explained later in this chapter on the basis of the Dalitz plots for the reactions. We will first discuss the di-pion mass spectra (Figure 9). The dashed curves show Lorentz invariant phase space (see Appendix A for the definition of this), and are normalized to the number of events, excluding those events inside the resonance peaks. The $\pi^{-}\pi^{\circ}$ mass spectrum shows a peak centered at 765 MeV which we attribute to the ρ-meson. The $\pi^{-}\pi^{+}$ mass spectrum shows a very strong peak also centered at 765 MeV and another peak centered at 1250 MeV which we attribute to ρ° and f°, respectively. The

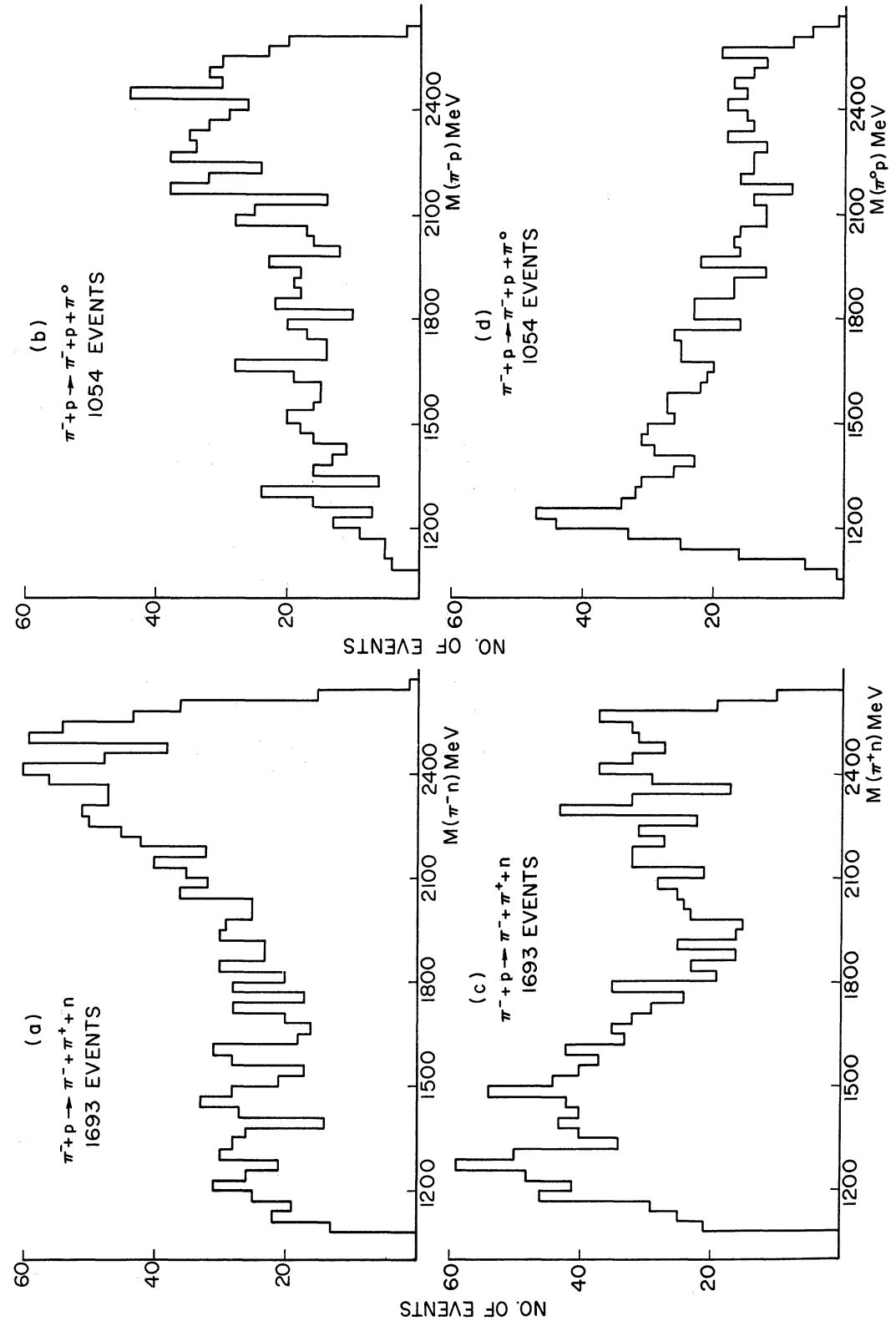

Figure 8. Effective mass distribution for pion-nucleon system.

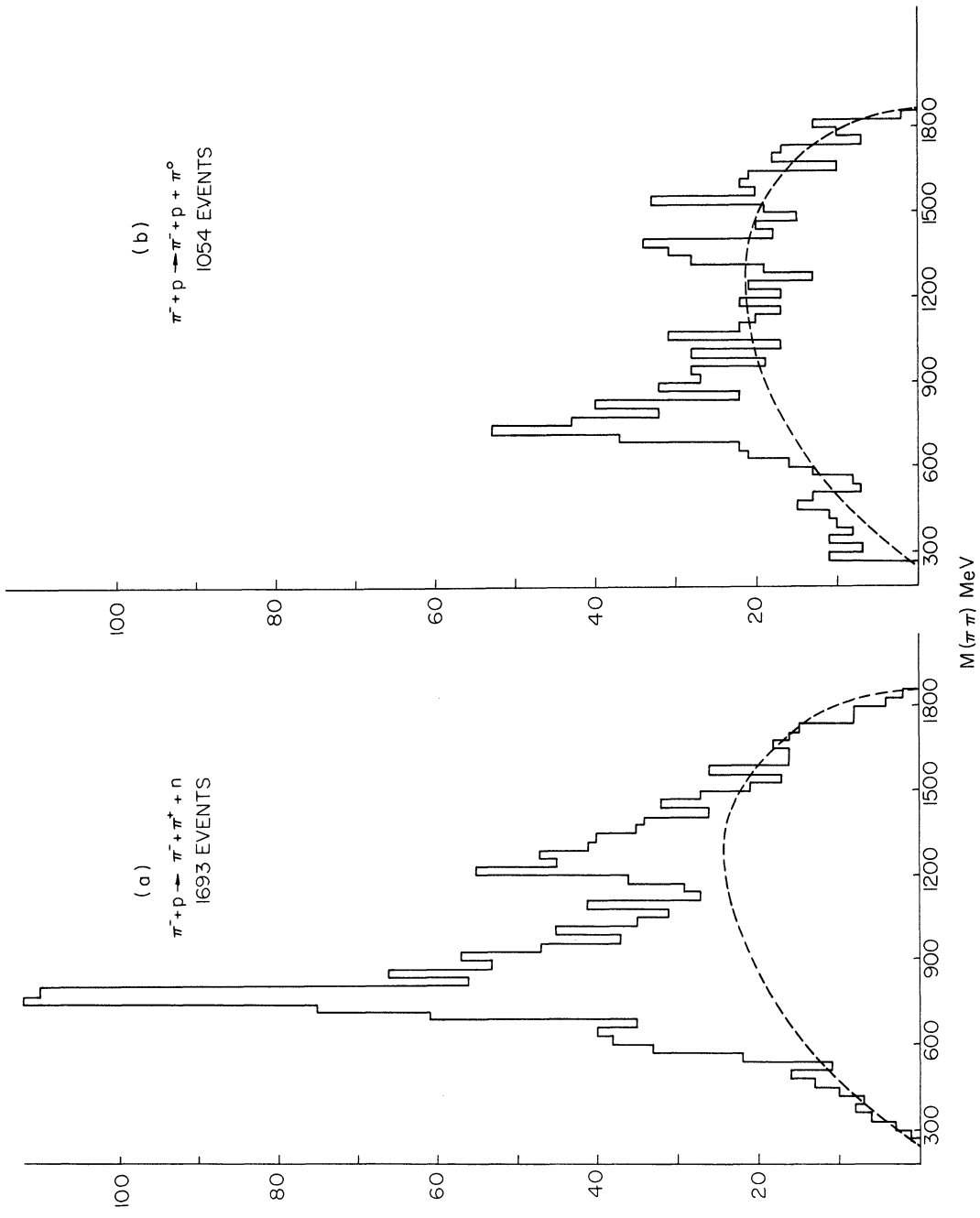

Figure 9. Effective mass distribution for pion-pion system.

The ρ's and f° have also been discovered by earlier workers.[7-11]

5.2.2 The Parameters of Resonances

An important characteristic of a resonance peak is its width. The estimation of the width at half maximum varies according to the assumed mathematical form of the resonance. We have estimated the width of these resonances by adopting a Breit-Wigner formula,[38]

$$H(M) = \frac{N\Gamma^2}{(M-M_0)^2+(\Gamma/2)^2}$$

where H is the height at the mass value M, M_0 is the value of M at the peak, N is a normalization factor, and Γ is the full width at half maximum. In interpreting our data we have also given an energy dependence to Γ according to[41]

$$\Gamma = Cp^3 = C'(M_{\pi\pi}^2-4m_\pi^2)^{3/2}$$

where C and C' are constants and p is the momentum of one of the pions in the di-pion system. We have used this form since it gives a better fit to our mass histograms. Below is a table of resonance peaks and width obtained in this experiment by trial and error which best fits the above formula for H(M) including the effect of background which follows phase space.

There seems to be a possible dependence of M_0 and Γ for our data on momentum transfer (Δ^2 defined later in this section). Figure 10 shows the histograms of $\pi^-\pi^+$ mass in reaction (3) around the region of ρ for those events which have $\Delta^2 < 4\mu^2(\mu = m_\pi)$ (Figure 10a) and those

TABLE III

THE RESONANCES AND THEIR WIDTHS

Name	M(MeV)	Γ(MeV)	Production Cross Section (mb)
ρ^-	765	125 ± 15	$0.33^{+0.2}_{-0.1}$
ρ°	765	125 ± 15	$1.02^{+0.3}_{-0.1}$
f°	1250	130 ± 20	$0.27^{+0.3}_{-0.1}$

with Δ^2 between $4\mu^2$ and $20\mu^2$ (Figure 10b). The dashed curves are fitted to the Breit-Wigner formula. Note that the width of the peak is considerably less than that of the combined data (Table III). We obtain about 80 MeV for Figure 10a and almost 90 MeV for the higher Δ^2 events in Figure 10b. The center of the peak of Figure 10b is also shifted by 30 MeV toward higher mass values. One possible explanation for this change of the width and the center value is that lower momentum transfer means the reaction is more peripheral so that the impact parameter of the reaction is bigger. Therefore, the resonance has less opportunity to interact with the nucleon field before or after it decays. Thus, interference from the nucleon field becomes smaller as Δ^2 becomes smaller. Such interference could be expected to increase Γ and also possibly cause a shift in M.

5.3 INTERPRETATION OF ρ PEAK AS PION-PION SCATTERING RESONANCE*

5.3.1 Production Mechanism

Chew and Low[17] have proposed a method to analyze the scattering

*Since the data process was delayed by various reasons, we used 1398 events for reaction (3) and 868 events for reaction (2).

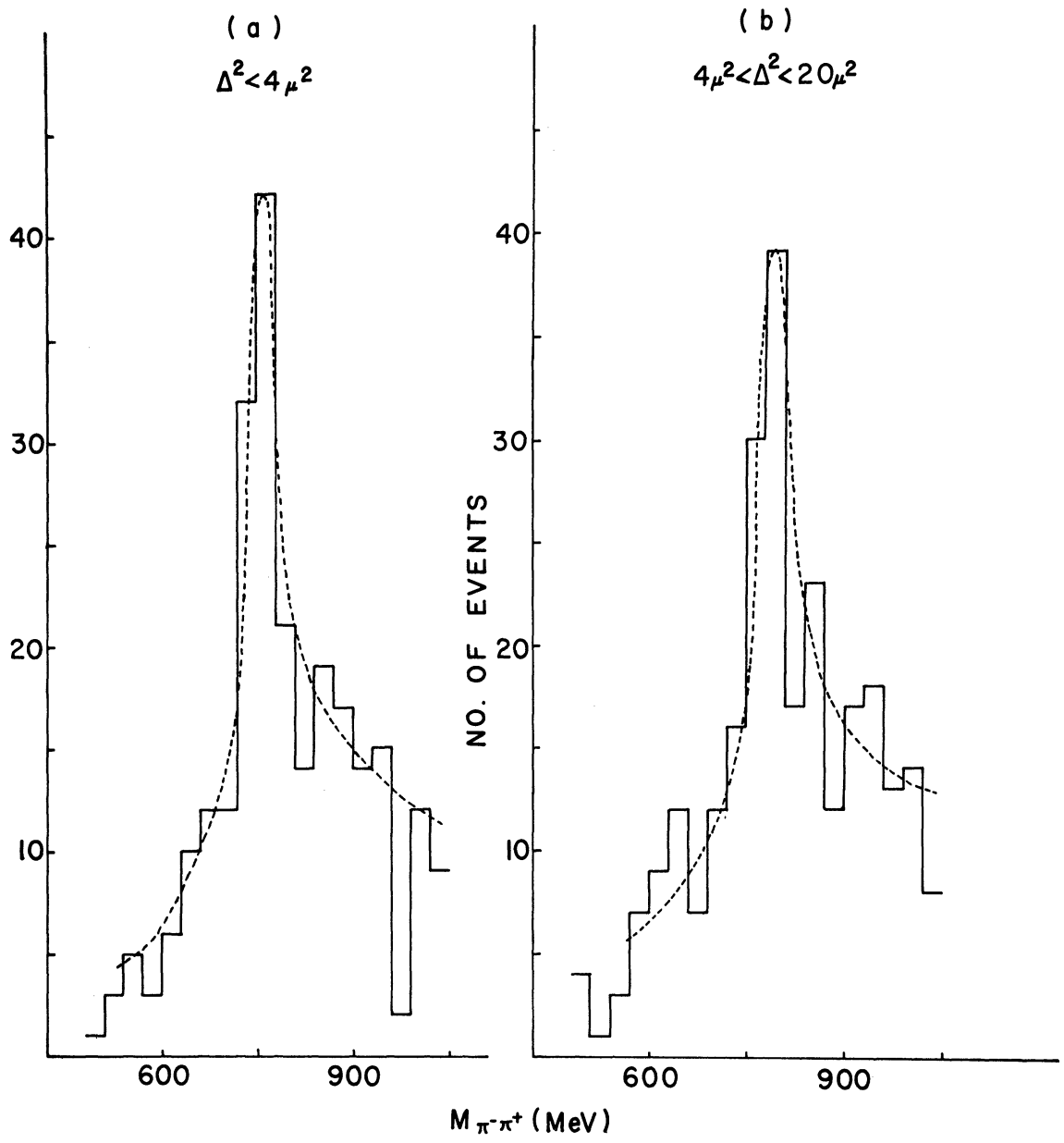

Figure 10. Effective mass distribution for pion-pion system for different Δ^2 regions.

process on a virtual target as a method by which to obtain information about scattering processes on unstable particle targets. In particular they have given an expression for the cross section on this virtual target. The process $\pi^-+p \rightarrow \pi+\pi+N$ with which we are dealing, could proceed through a one-particle exchange diagram, illustrated in Figure 13. Therefore the Chew-Low idea should be applicable to this experiment. If the process proceeds through one pion exchange, the scattering amplitude has an isolated pole in the nonphysical region at $\Delta^2 = -\mu^2$, where Δ^2 is the four-momentum transfer from the target proton to the recoil nucleon (or incident pion to final di-pion system). It is given by

$$\Delta^2 = (P_i - P_o)^2$$

where P_i and P_o are the four-momentum of the initial and outgoing nucleons. The value of Δ^2 is Lorentz invariant and is given in the laboratory system by twice the mass times the kinetic energy of the outgoing nucleon. We take μ (equals the pion mass) as the unit of four-momentum transfer. According to Chew and Low, the pion-nucleon cross section is expressed in terms of the pion-pion cross section as

$$\frac{d^2\sigma_{\pi p}}{dM_{\pi\pi}^2 d\Delta^2} = \lim_{\Delta^2 \rightarrow -1} \frac{f^2}{2\pi} \frac{\Delta^2}{(\Delta^2+1)^2} \frac{M_{\pi\pi}\left(\frac{M_{\pi\pi}^2}{4} - 1\right)^{1/2}}{P^2_{\text{beam in lab.}}} \sigma_{\pi\pi}(M_{\pi\pi}^2)$$

where f^2 is pion nucleon coupling constant. Therefore, in the physical region the interaction is characterized by strong enhancement at small values of the Δ^2 and this can be used as a test to see whether the interaction appears to be peripheral and consistent with one pion ex-

change.

Figure 11 shows the scattergram of Δ^2 versus $M^2_{\pi\pi}$ (Chew-Low plot). Here one can see that most of the events are in the lower part, especially for the resonances. The concentration of the dots around the $M^2_{\pi\pi}$ of 0.68 BeV^2 is due to the ρ's and another around 1.56 BeV^2 represents the f° resonance. There are very few events with momentum transfer of more than $20\mu^2$. Figure 12 shows the distribution of Δ^2 for those events inside the three resonances. The plot is only for $\Delta^2 < 50\mu^2$ because only a few events remain after that point. The first few depleted bins for the f° show the phase space limitation for this mass region, i.e., the kinematics impose a lower limit on Δ^2 for a given $M_{\pi\pi}$, which at the f° mass is $2.6\mu^2$. In all these distributions, we note that most of the events are confined to less than $20\mu^2$ of momentum transfer. The evidence given by Figures 11 and 12 is consistent with the reactions being peripheral, and proceeding through one particle exchange.

The only known particle that can be exchanged in the ρ° case is the π^+, while the ρ^- case can have π° and ω°, provided that only strong interactions contribute to these reactions. Below are the exchange diagrams for these reactions.

Treiman and Yang have suggested a way of testing the one-particle exchange mechanism.[32] If the exchange particle is spinless (like the pion) there should be no preference of azimuthal angle around the exchange particle direction because a spinless particle cannot transmit any directional information. This azimuthal angle can be calculated in

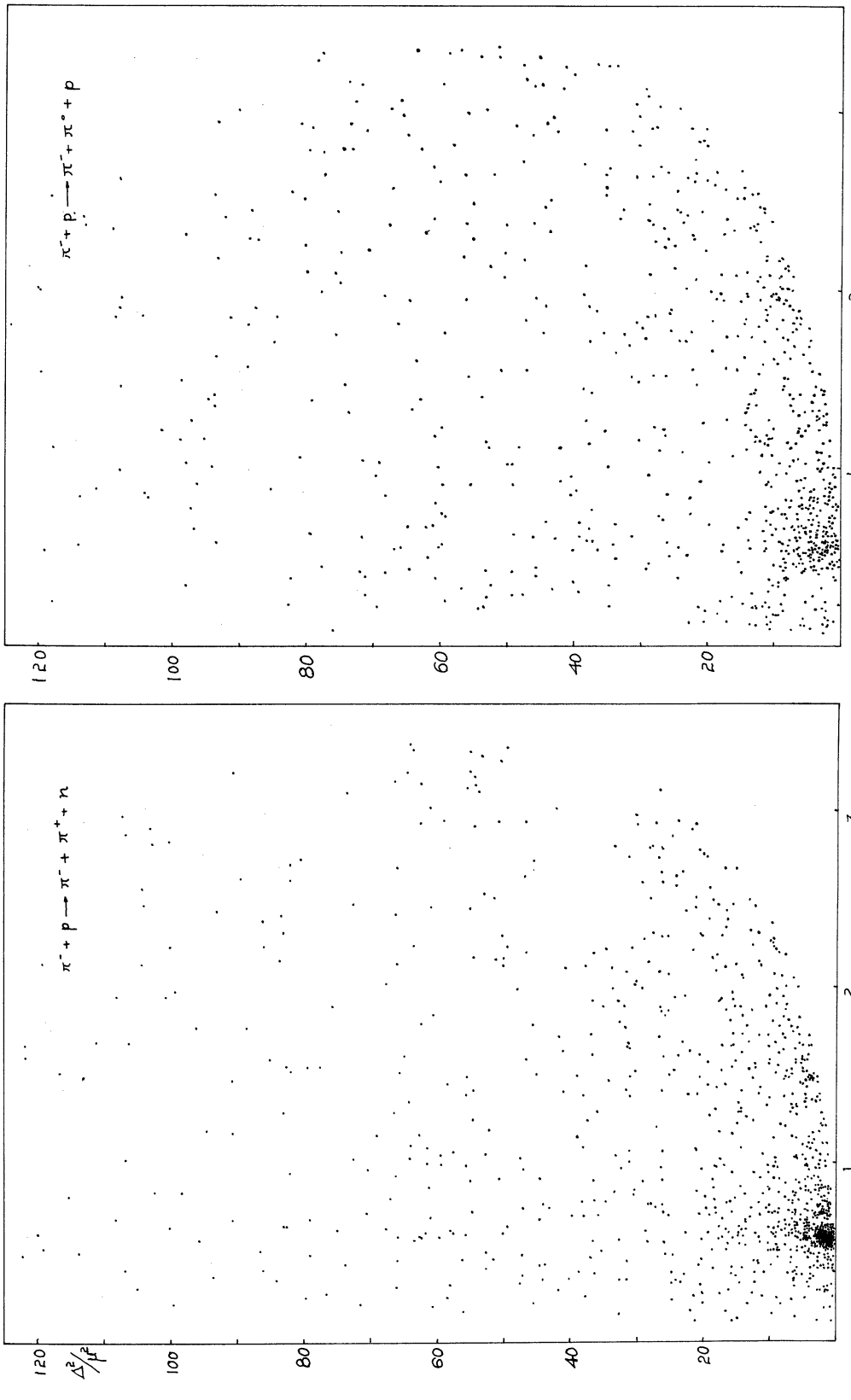

Figure 11. Chew-Low plot of 4-momentum transfer.

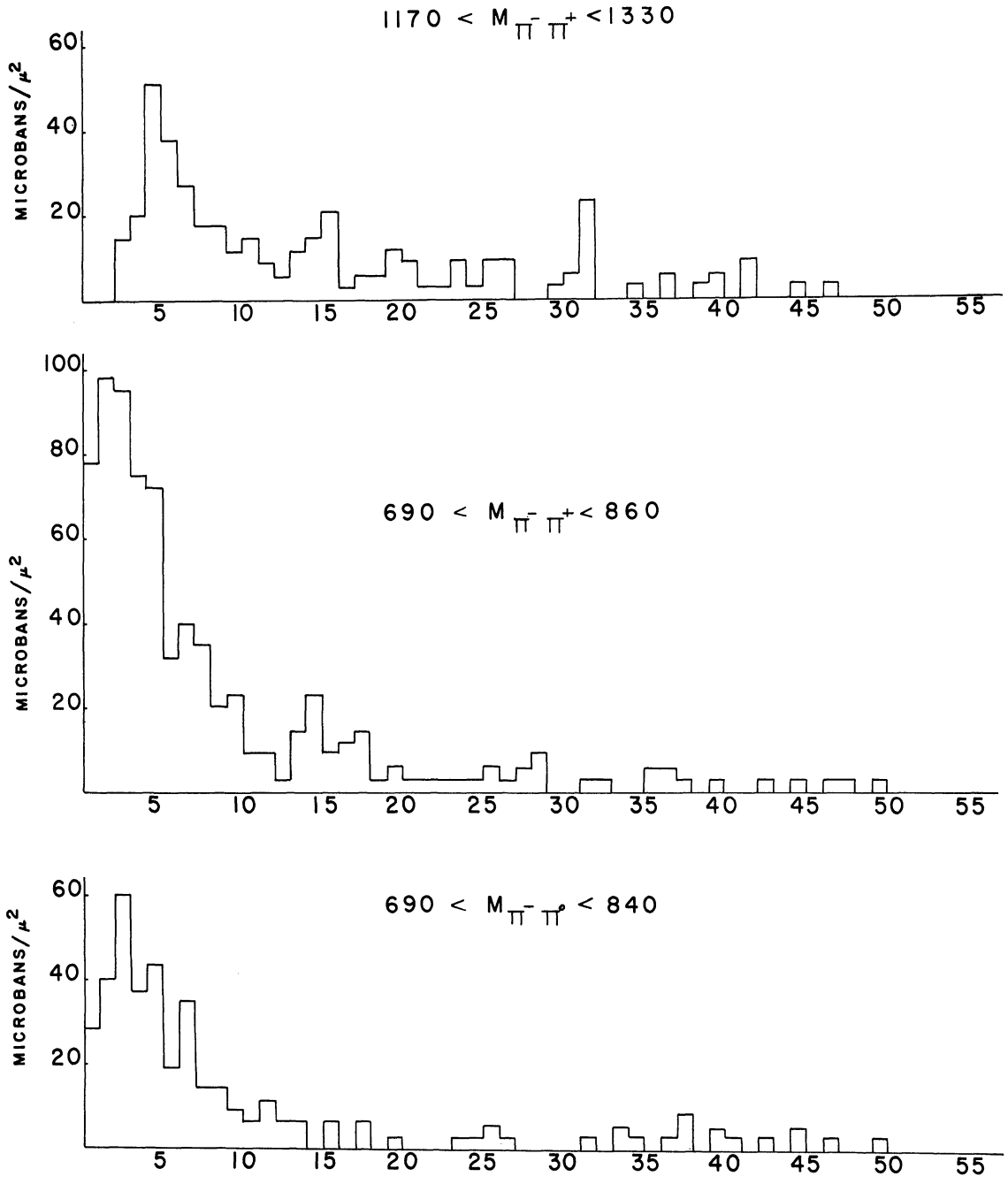

Figure 12. Four-momentum transfer distribution for ρ's and f°.

the rest frame of the incident pion by

$$\cos(TY) = \frac{(P_1 \times P_2) \cdot (P_3 \times P_4)}{|P_1 \times P_2| \, |P_3 \times P_4|}$$

where P_1, P_2, P_3, and P_4 are the 3-momenta of the target particle, recoiled nucleon and two outgoing pions. Since we are dealing with strong interactions in which parity is conserved at each vertex, we can fold the distribution about 180° line. The reason for this is that the reaction must be independent of spatial inversion which changes the direction of all momenta, and therefore changes the sign of the T-Y angle (but not of its cosine).

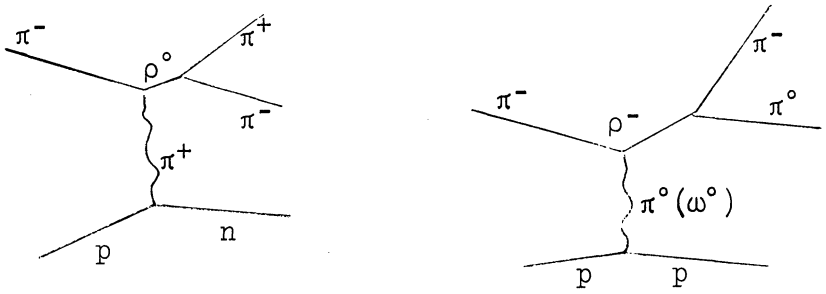

Figure 13. One-particle exchange diagrams for ρ production.

Figure 14 shows scattergrams for this angle, taking four-momentum transfer in the vertical direction. We note that all those are consistent with isotropy except for a slight depopulation at higher values of the T-Y angle. One can conclude that one pion exchange cannot be excluded by this test.

In Figure 14b, one might notice, besides the depopulation for higher values of the T-Y angle, that there is depopulation around 0°. This depopulation might be caused by those events which exchanged an ω. This fact contradicts our assumption of a one-pion exchange model. An-

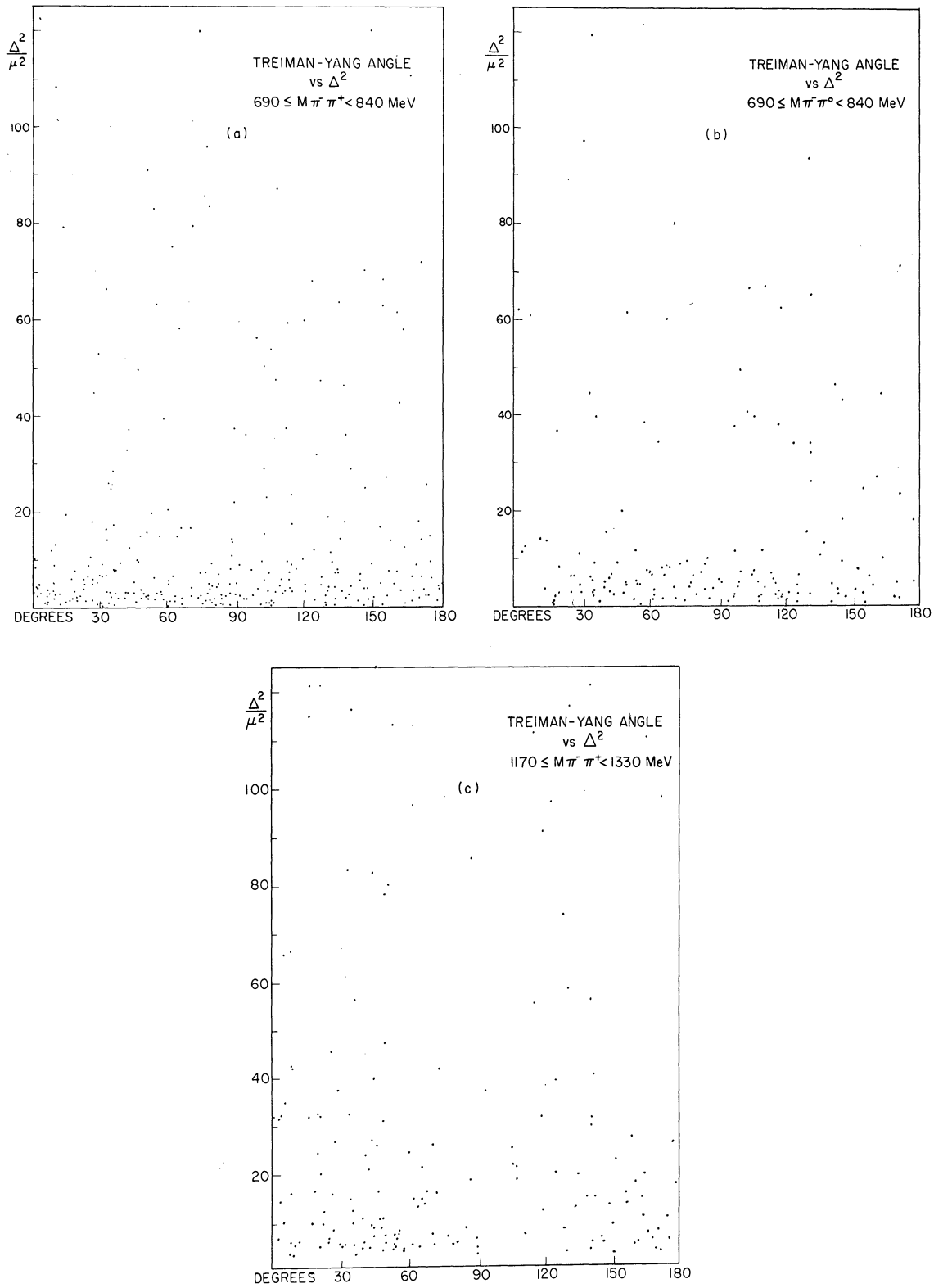

Figure 14. Treiman-Yang angle distribution for ρ's and f°.

other discrepancy for the one-pion exchange model is that the production ratio of ρ^- and ρ^0 given in Table III is about 1 to 3 whereas it should be 1 to 2 for one-pion exchange. The ratio 1 to 2 comes from analysis similar to that given in Appendix B. Thus one might doubt the one-pion exchange assumption; however, this will be explained in the next section by looking at decay angular distributions.

5.3.2 Decay Angular Distribution of ρ

Let us now concentrate our attention on the ρ resonances. The quantum numbers are T = 1, 1^{-+}(J^{parity}, G-parity) as shown by earlier workers.[7-9] As was shown before, the production of the ρ is consistent with one-meson exchange dominating the reactions. Assuming that the one-meson exchange hypothesis is correct at least for the major portion of the events, let us study the decay angular distribution of the ρ-meson. We define the angle θ between incoming and outgoing π^- in rest system of final di-pion (Figure 15).

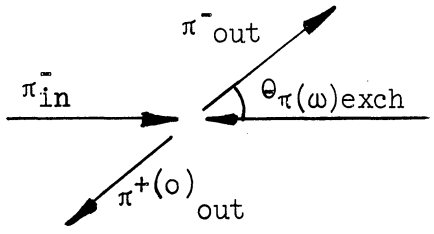

Figure 15. Space diagram of pion vertex in rest frame of final di-pion system.

As stated before, the only possible particles which could be exchanged in these reactions are either the pion or the ω. Therefore, the distribution of events should go as $\cos^2\theta$ for pion exchange and $\sin^2\theta$ for ω exchange provided there are no final state interactions or

interference from other production mechanisms (see Appendix C). However, none of the angular distributions shows either of these predicted distributions (Figure 16). Assuming the peripheral interaction to be characterized by low-momentum transfer, we took events with momentum transfer less than $20\mu^2$ in Figure 16. One can notice a strong forward-backward asymmetry in the ρ° decay angular distribution, indicating the strong presence of odd powers of cos θ. The ρ° does not seem to have such an asymmetry.

5.3.3 Possible Explanation of Asymmetry in ρ°

We can think of several reasons which might explain the heavy asymmetry in ρ° decay angular distribution. They are (a) interference effects from nucleon isobar formation,[33] (b) possible interference from the two-pion decay of ω-meson,[34] and (c) interference between the resonance and possible s-wave background, along with off-energy shell effects due to the fact that the struck pions are "virtual."

As will be seen later from the Dalitz plots (Figure 22) the effects due to isobar formation, if any, are very small. The effect due to the possible two-pion decay of ω-meson is hardest to estimate, although it should not be very large due to the fact that this decay violates G-parity and cannot be a strong interaction. The sharp peak of ρ° (Figure 9a) and the shifted peak for those events having different momentum transfer (Figure 10) might be due partly to two-pion decay of the ω-meson. However, this might also be caused by secondary interactions

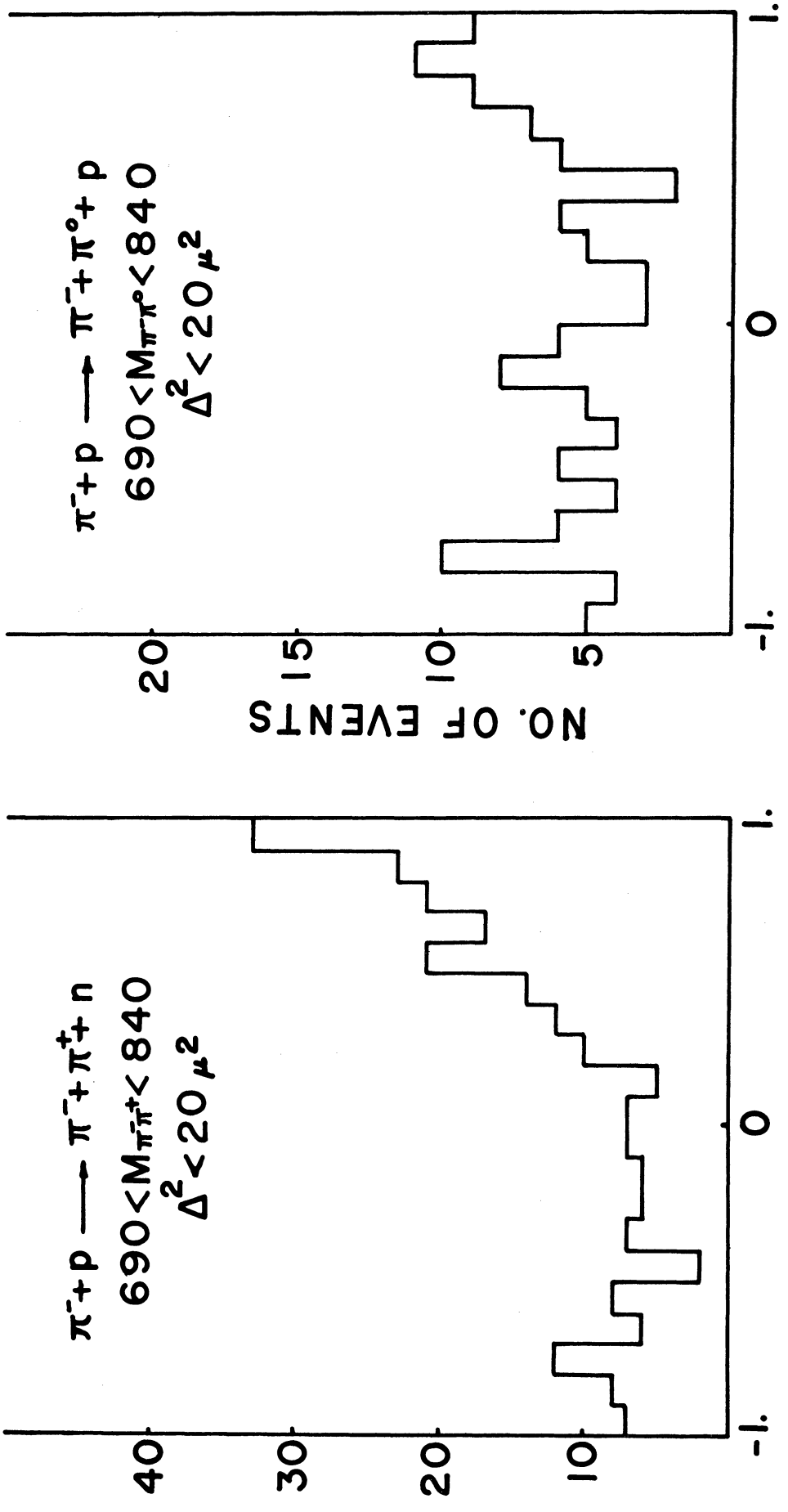

Figure 16. Distribution for cos θ inside the ρ-meson region.

with the nucleon field, the effects of which are too hard to estimate at this stage. In any case, we will neglect these effects and proceed to discuss the third reason, which seems to give a good explanation for the cos Θ asymmetry.[12,18]

We want to make an empirical fit to the cos Θ distribution by means of a partial wave analysis for pion-pion scattering. The two pions can be in the T = 0, 1, or 2 states of isotopic spin. Because of the generalized Pauli principle, even T states can only be accompanied by even angular momentum, and likewise, for odd T, only odd J is allowed. The simplest case would be a mixture of a T = 0, L = 0 state with a T = 1, L = 1 state, assuming T = 2 terms and higher angular momentum terms are negligible. The absence of a T = 2 state will be verified later in this chapter. The ρ° asymmetry can arise due to the quantum-mechanical interference of these two states. The lack of asymmetry in the ρ^{-} case is then understandable also, since T = 0 is not allowed for the $\pi^{-}\pi^{\circ}$ system.

The partial wave expression for the cross section which contains only T = 0, L = 0 and T = 1, L = 1 terms is given by

$$\frac{d\sigma_{\pi\pi}}{d(\cos\Theta)} = \frac{1}{k^2}\left|\frac{2}{3}e^{i\delta_{0,0}}\sin\delta_{0,0} + 3e^{i\delta_{1,1}}\sin\delta_{1,1}\cos\Theta\right|^2$$

$$= \frac{1}{k^2}\left(\frac{4}{9}\sin^2\delta_{0,0} + 4\sin\delta_{0,0}\sin\delta_{1,1}\cos(\delta_{0,0}-\delta_{1,1})\right.$$

$$\left. \times \cos\Theta + 9\sin^2\delta_{1,1}\cos^2\Theta\right)$$

$$= A + B\cos\Theta + C\cos^2\Theta$$

where

$$A = \frac{4}{9k^2} \sin^2\delta_{0,0} \quad B = \frac{4}{k^2} \sin\delta_{0,0} \sin\delta_{1,1} \cos(\delta_{0,0}-\delta_{1,1})$$

and

$$C = \frac{9}{k^2} \sin^2\delta_{1,1} \quad .$$

The phase difference between s- and p-wave can be calculated by

$$\cos(\delta_{0,0}-\delta_{1,1}) = B/2\sqrt{AC}$$

where $\delta_{0,0}$ and $\delta_{1,1}$ are the phase shifts for s- and p-wave, respectively, and k is the pion-pion center-of-mass momentum and we take units such that $\hbar = 1$. It is expected that the phase shifts will depend on the total energy ($M_{\pi\pi}$) which, of course, is simply related to k. The factor 2/3 in front of the s-wave term comes from the following argument. The wave function of the incoming di-pion system can be expressed in terms of its isotopic spin components as

$$\psi(\pi^-\pi^+) = \sqrt{\frac{1}{3}}\,\psi_0 + \sqrt{\frac{1}{2}}\,\psi_1 + \sqrt{\frac{1}{6}}\,\psi_2$$

where the indices for ψ denote the isotopic spin of the two-pion system, and the constants are the Clebsh-Gordon coefficients.[30] The functions ψ can be expressed in terms of the products of the single pion isospin functions as

$$\psi_0 = \sqrt{\frac{1}{3}}\left(\pi^-(1)\pi^+(2)+\pi^+(1)\pi^-(2)-\pi^\circ(1)\pi^\circ(2)\right)$$

$$\psi_1 = \sqrt{\frac{1}{2}}\left(\pi^-(1)\pi^+(2)-\pi^+(1)\pi^-(2)\right)$$

$$\psi_2 = \sqrt{\frac{1}{6}}\left(\pi^-(1)\pi^+(2)+\pi^+(1)\pi^-(2)+2\pi^\circ(1)\pi^\circ(2)\right) \quad .$$

Therefore, the final state wave function can be written in terms of the scattering amplitude (A_T) for the three T-states as

$$\psi_f = \frac{A_0}{3}(\pi^-\pi^+ + \pi^+\pi^- - \pi^\circ\pi^\circ) + \frac{A_1}{2}(\pi^-\pi^+ - \pi^+\pi^-)$$

$$+ \frac{A_2}{6}(\pi^-\pi^+ + \pi^+\pi^- + 2\pi^\circ\pi^\circ) \quad .$$

This can be written as

$$\psi_f = \left(\frac{\sqrt{2}}{3}A_0 + \frac{\sqrt{2}}{6}A_2\right)\left(\frac{\pi^-\pi^+ + \pi^+\pi^-}{\sqrt{2}}\right) + \left(\frac{A_1}{\sqrt{2}}\right)\left(\frac{\pi^-\pi^+ - \pi^+\pi^-}{\sqrt{2}}\right)$$

$$+ \left(-\frac{A_0}{3} + \frac{A_2}{3}\right)(\pi^\circ\pi^\circ) \quad .$$

The coefficient of the first term represents the amplitude for observing $\pi^-\pi^+$ in an L = even state, the second is for $\pi^-\pi^+$ in an L = odd state and the third for observing two π°'s. Since we observe in this experiment an outgoing $\pi^-\pi^+$ but do not determine its L-value we must use $\frac{\sqrt{2}}{3}A_0 + \sqrt{\frac{1}{2}}A_1$ as our amplitude (we take $A_2 = 0$ as mentioned previously). The relative strength of the A_0 to A_1 amplitude is therefore 2/3, as indicated in the phase shift formula. The factor 3 in front of the $e^{i\delta_{1,1}}\sin\delta_{1,1}$ term is the (2L+1) factor in the partial wave expansion of the A's in terms of the Legendre polynomials.

Since the ρ^- case does not have as large a asymmetry as the ρ°, we conclude that there is either no T = 2 s-wave or, if any, it is very small or incoherent.

For the ρ° case we have fitted the angular distributions to $A+B\cos\theta+C\cos^2\theta$. Figure 17 shows the cos θ distributions for various $M_{\pi\pi}$ regions and for Δ^2 less than $20\mu^2$. The dashed curves represent the fitted curves as determined by a least squares program, and are normalized to the proper number of events in each case. Below is the table for the coefficients A, B, and C along with $B/2\sqrt{AC}$ and the χ^2 probability. The coefficients, A, B, and C are normalized to arbitrary units in Table IV. The term $B/2\sqrt{AC}$ would be the cosine of the difference of the s- and p-wave phase shift angles if the target were a real particle. In Figure 18 we have plotted the results of Table IV. The number in Figure 18 is normalized the same way as in Table IV. Figure 18c shows

TABLE IV

LIST OF FITTED COEFFICIENTS AND χ^2 PROBABILITY FOR DIFFERENT DI-PION MASS

Mass Region, M		A	B	C	$B/2\sqrt{AC}$	χ^2 Probability
590	690	0.87	0.43	1.12	0.24	15 (%)
690	740	1.31	3.47	4.44	0.72	64
740	790	2.91	6.60	7.90	0.73	29
790	840	2.03	2.14	4.88	0.33	44
840	940	2.14	1.06	2.82	0.21	15
940	1040	0.79	0.16	2.71	0.04	3

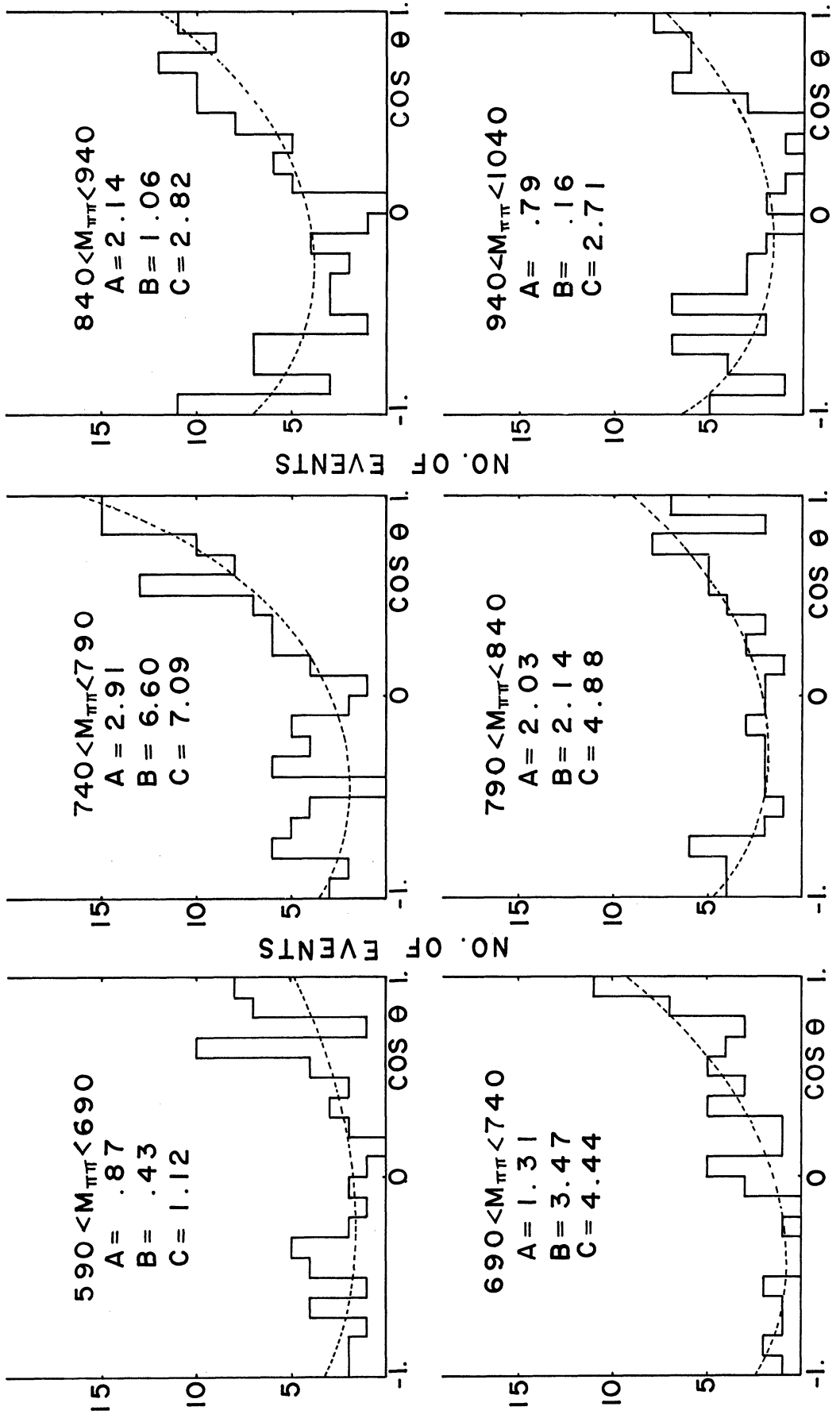

Figure 17. Distribution of cos θ for different $\pi^-\pi^+$ mass and for $\Delta^2 < 20\mu^2$.

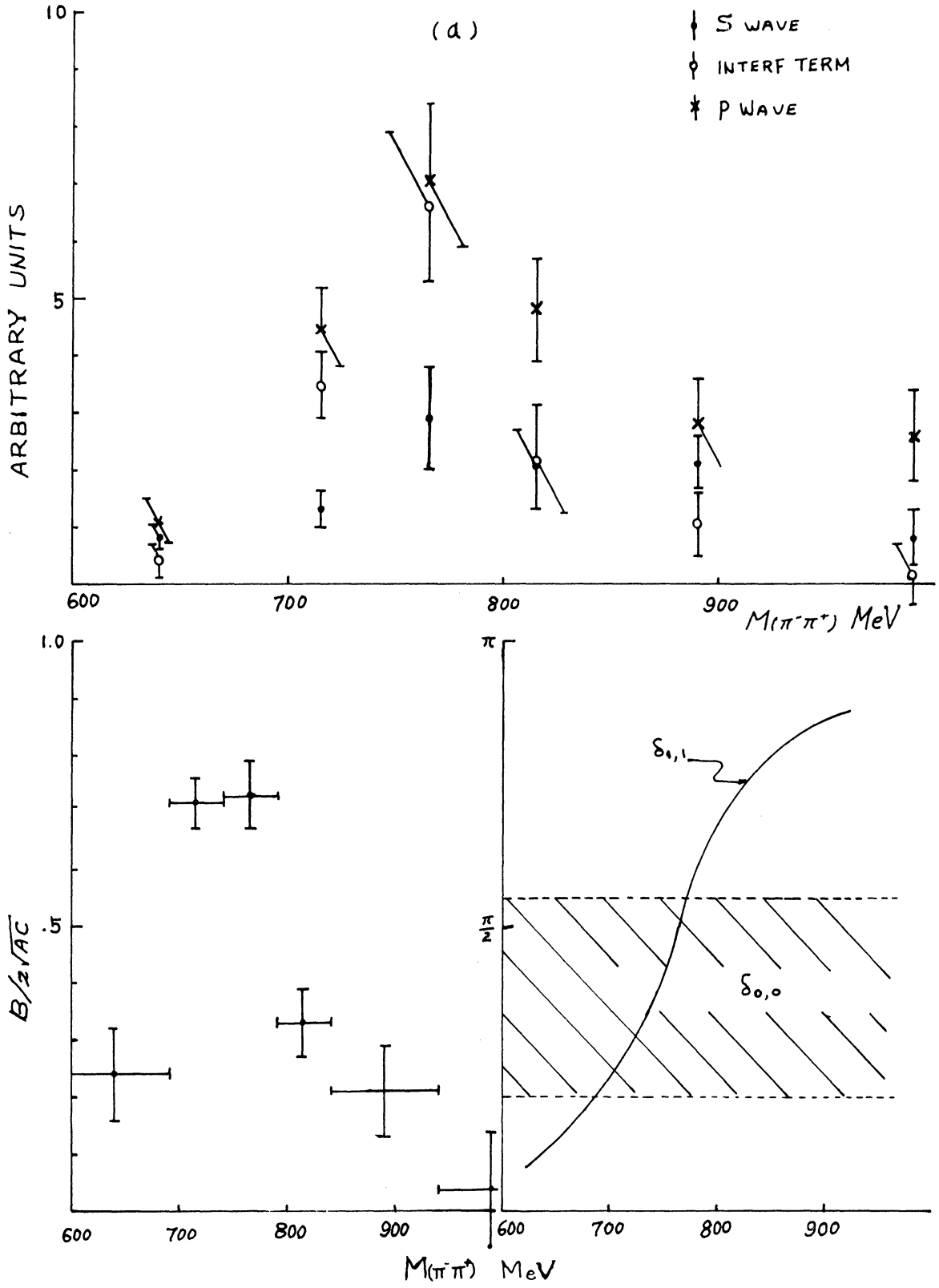

Figure 18. Coefficients A, B, and C with $B/2\sqrt{AC}$ and possible phase-shift diagram.

the energy dependence of the phase shifts assuming the p-wave phase shift propagates from 0° to 180° across the resonance. The s-wave phase shift remains approximately constant and large $(75\pm35)^\circ$ throughout the region. This value of $75^\circ\pm35^\circ$ was obtained from Figure 18b by assuming $\cos(\delta_{0,0}-\delta_{1,1}) = B/2\sqrt{AC}$ and taking $\delta_{1,1}$ by the Breit-Wigner resonance formula. As one can see from Table IV and Figure 18, the s-wave amplitude remains almost constant, as would be expected. The slight increase of the s-wave amplitude at the ρ° mass might be statistically not significant and we are not able to conclude if this effect is real or not. The p-wave and interference terms definitely show a sudden increase in their coefficients at the resonance region. Figure 18b shows the $B/2\sqrt{AC}$ term which also peaks near the resonance. All these effects are consistent with the dependence shown in Figure 18c.

Since the target is not a real pion, we are not able to interpret these values of the phase shifts as being quantitatively correct, but qualitative agreement with our form for the partial wave expansion is very encouraging. An attempt to make these results quantitative will be given in the next section.

Thus our interpretation seems to be justified that the ρ is a p-wave resonance of pion-pion scattering with the forward-backward asymmetry being caused by interference with the s-wave background. However, there is one point which is bothersome. We notice from Table IV that the ratio of C to A is always less than 3 to 1, whereas if the

phase shifts behave according to Figure 18c the ratio should be 81 to 4, or about 20 to 1, near the peak. The ratio 81 to 4 is obtained from the expression for A and C by setting $\delta_{0,0} = \delta_{1,1}$. We will see in the next section that this ratio becomes much closer to its expected value when we extrapolate A, B, C to the value $\Delta^2 = -1$.

5.3.4 Extrapolation Into the $\Delta^2 = -1$ Pole

One can think of several possible explanations for the discrepancy in the ratio of the s- and p-wave amplitude. The most plausible are: (a) the estimation of A, B, C at the peak is an average value over some finite interval of pion-pion mass hence one does not get the maximum peak value for the p-wave; and (b) the off-energy shell effect makes the quantitative results unreliable. The first explanation gives a small effect, of order 10%, but cannot take care of the whole discrepancy. For an investigation of the second explanation we have to extrapolate the s- and p-wave amplitudes into the nonphysical region, i.e., to $\Delta^2 = -1$. Figure 19 is the angular distribution in the various Δ^2 regions for the entire ρ region ($690 < M_{\pi\pi} < 840$ MeV). The coefficients A, B, and C for each division are shown in Table V. The coefficients A, B, and C are normalized to the number of events. The value for Δ^2 from 20 to infinity is not reliable because of a large χ^2 value (or small probability) and too big Δ^2 interval. It is clear that the ratio C/A is rapidly increasing as Δ^2 decreases. In order to use these coefficients in the Chew-Low formula we must convert them into values

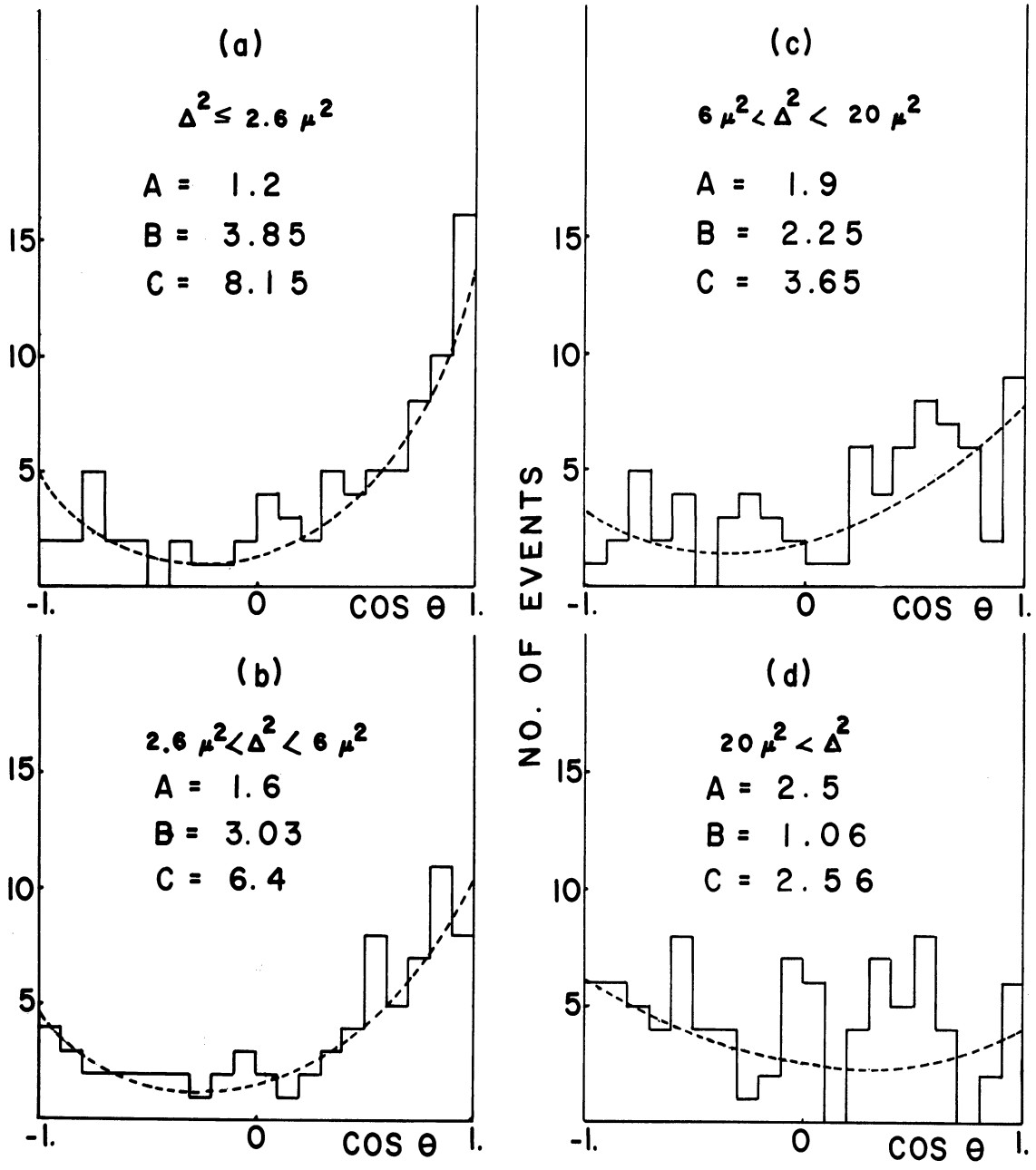

Figure 19. Distribution for cos θ for different Δ^2 for the events inside the ρ°-region.

TABLE V

LIST OF FITTED COEFFICIENTS AND χ^2 PROBABILITY FOR DIFFERENT Δ^2

Δ^2/μ^2 Region	A	B	C	C/A	χ^2 Probability
0.0 - 2.6	1.20	3.85	8.15	6.80	75 (%)
2.6 - 6.0	1.60	3.03	6.40	4.00	80
6.0 - 20.0	1.90	2.25	3.65	1.92	22
20.0 - infinity	2.50	-1.06	2.56	1.02	0.1

per unit Δ^2 interval by dividing by the difference of Δ^2. In order to convert into values per unit steradian we actually divided by

$$d\Omega = -2\pi d(\cos\alpha) = -\frac{\pi d\Delta^2}{P_{beam}P_\rho}$$

where α is the ρ production angle and the values of P_{beam} and P_ρ (which is practically constant) are taken in the center-of-mass system of the whole reaction. As suggested by Selleri[36] we make use of the modified Chew-Low formula (all in pion mass units)

$$\frac{d^3\sigma(\pi p \to p\rho)}{d\Delta^2 d\omega^2 d\Omega'} = \xrightarrow[\Delta^2\to -1]{} \frac{f^2}{\pi}\frac{\Delta^2}{(\Delta^2+1)^2}\left(\frac{\Lambda^2-1}{\Lambda^2+\Delta^2}\right)^2 \frac{\omega k_1}{k_{1L}}\frac{d\sigma(\pi\pi \to \pi\pi)}{d\Omega'}$$

where $(\Lambda^2-1)/(\Lambda^2+\Delta^2)$ is a phenomenological form factor which is unity at the $\Delta^2 = -1$ pole, f^2 is the pion-nucleon coupling constant, k_1 and k_{1L} are the momentum of incoming particle in the rest system of di-pion and the laboratory system, respectively. The symbol Ω' represents the solid angle for the outgoing π^- in the rest frame of the di-pion, and ω is the effective mass of the di-pion system. One then multiplies the coefficients A, B, and C by the factor of $((\Delta^2+1^2)^2/\Delta^2)\cdot((\Lambda^2+\Delta^2)/(\Lambda^2-1))^2$ which is the inverse of the factor in the above equation. The free param-

eter Λ^2 was determined from the overall Δ^2 distribution and is $6\mu^2$. Figure 20 is a plot of ((A,B,C)/sr). $((\Delta^2+1)^2/\Delta^2)((\Lambda^2+\Delta^2)/(\Lambda^2-1))^2$ and a possible extrapolation to $\Delta^2 = -1$ in the nonphysical region. The extrapolated values for A, B, and C are 0.76 ± 0.4, 5.9 ± 0.9, and 14.1 ± 1.9 mb/sr, and the ratio C/A comes to about 20 which is now in excellent agreement with the predicted value (see Section 5.3.3).

We can also make a calculation of the s-wave phase shift from

$$\frac{B}{C} = \frac{4}{9} \frac{\sin \delta_{0,0} \sin \delta_{1,1}}{\sin^2 \delta_{1,1}} \cos(\delta_{1,1}-\delta_{0,0}) \quad .$$

At the center of resonance we take $\delta_{1,1} = \pi/2$, then

$$\frac{B}{C} = \frac{4}{9} \sin^2 \delta_{0,0} = 0.42 \pm 0.11$$

which gives

$$\sin^2 \delta_{0,0} = 0.95 \pm 0.25 \quad .$$

This value for $\delta_{0,0}$ is consistent with the value shown in Figure 18c as determined in Section 5.3.3.

Professor Marc Ross has suggested to us that using this cross section for the p-wave (C term), we can calculate the pion-nucleon coupling constant (f^2) by using the measured ρ width to compute $\frac{d\sigma(\pi\pi\to\pi\pi)}{d\Omega'}$. We have done this[39] and obtained the value 0.103 ± 0.02, in good agreement with other determinations of f^2. Thus all this evidence agrees remarkably well with the assumption that the ρ° is a p-wave resonance of pion-pion scattering with s-wave background interference and with the phase

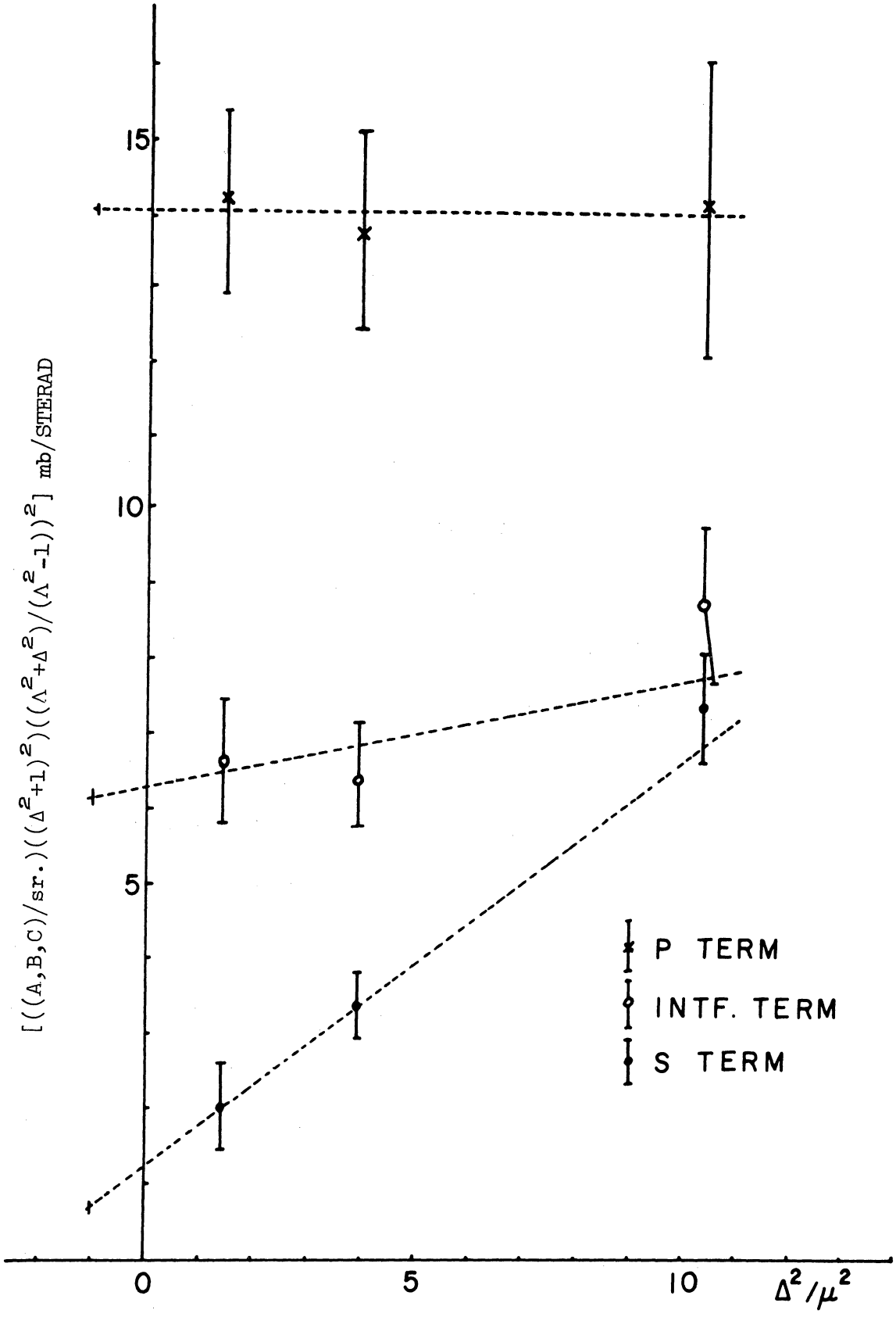

Figure 20. Extrapolation of partial wave amplitude to $\Delta^2 = -1$.

shift behavior being roughly that shown in Figure 18c.

5.3.5 Discussion of ρ^- Peak

Now let us turn our attention to the ρ^- decay angular distribution. In this case we cannot have as good an analysis as we had for the ρ° because of the more meager statistics. Figure 16 does not give too much promise of deciding whether an ω or a pion is exchanged, since the distribution must be $\sin^2\theta$ or $\cos^2\theta$, respectively, for these two possibilities. We investigate this question further by dividing the events into several Δ^2 regions and fitting each region separately. Figure 21 shows these angular distributions for ρ^- events ($690 < M_{\pi\pi} < 840$ MeV). One notices that Figure 21a and 21b do not have the shape of a $\sin^2\theta$ or $\cos^2\theta$ distribution. However, Figure 21c shows a more clear dependence of a $\cos^2\theta$ distribution and does not show the strong asymmetry we had for the ρ°, in agreement with the fact that there can be no s-wave mixture in the ρ^-. As in Figure 19, the dashed curve shows the fitted curve for a p-wave coefficient of 4.85, which was normalized to the number of events in Figure 21c. The slight asymmetry here might be an interference due to some $T = 2$, s-wave. However, we believe the more reasonable possibility is that it is due to $\pi^\circ p$ isobar formation. In fact the subtraction of possible isobar events (as determined from the Dalitz plot) removes the asymmetry. A justification of this isobar subtraction (the shaded area in Figure 21c) will be given in the next section. The method of subtraction is to randomly take out a constant

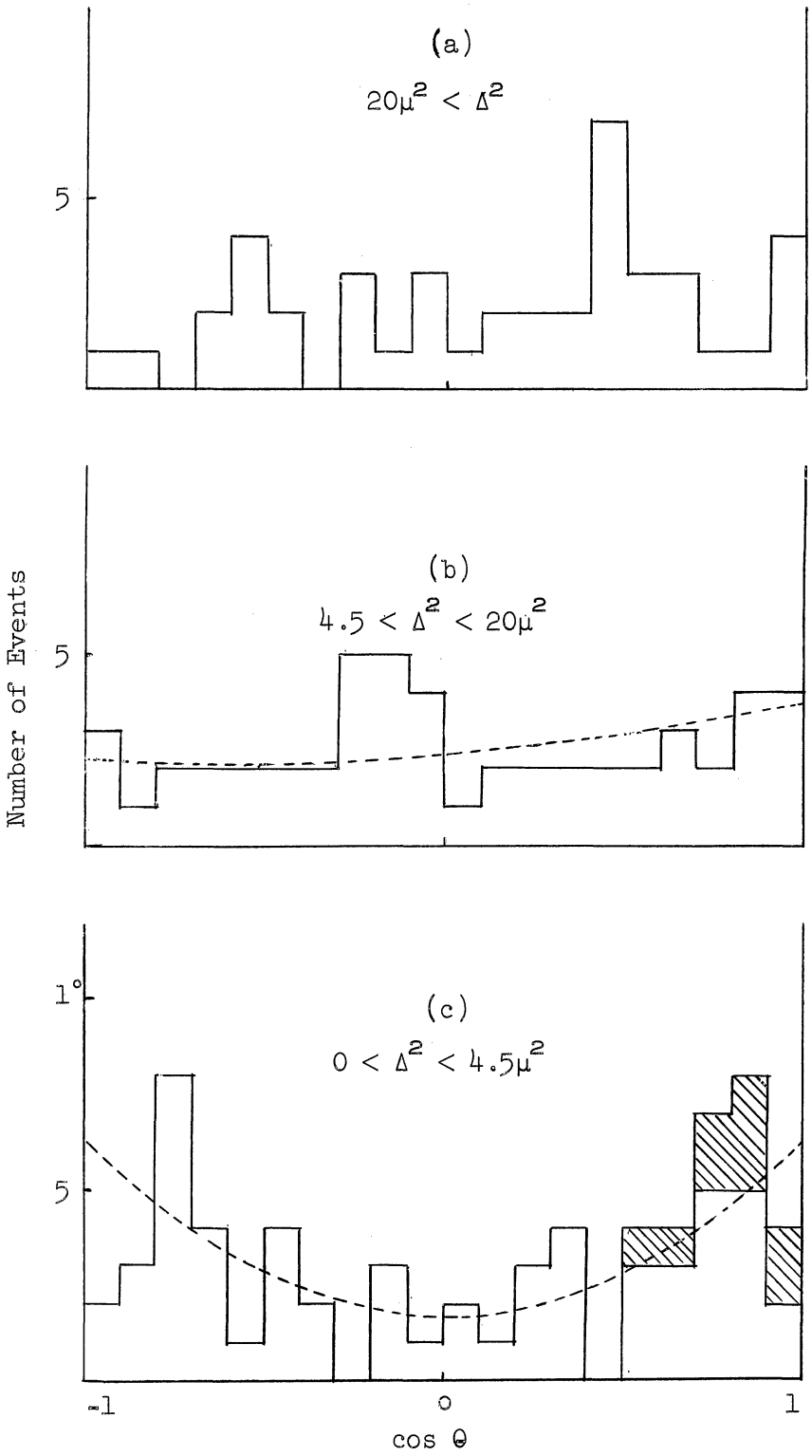

Figure 21. Distribution of cos Θ for the events inside the ρ^--region.

density of events along the N* band in the Dalitz plot, and this amounts to nine events. Thus for those events with momentum transfer less than $4.5\mu^2$, it appears that a substantial part of the reaction is going through one-pion exchange. The rather isotropic distribution in Figures 21a and 21b may be caused by ω exchange mixed with pion exchange or it may be that at higher Δ^2 the reaction does not go through a peripheral mechanism.

Now, if the ρ is a p-wave resonance then in ρ production via one-pion exchange there should exist a 2 to 1 ratio between ρ° and ρ^-. If we take our observed p-wave coefficient for the ρ^-, which is 4.85, and convert this number through the same procedure as we did for the ρ°, we obtain the value 6.7 ± 1.4 mb/sr. Since the p-wave part in the extrapolation (Figure 20) stays constant throughout the Δ^2 region (14.1 mb/sr) we can compare the above two numbers as representing their extrapolated values. This gives good agreement with the ratio 2:1, and resolves the discrepancy noted in Section 5.3.1.

5.4 DALITZ PLOTS AND ISOBAR FORMATION

We next discuss the question of nucleon isobar formation and the possible effects of this on the ρ and f° resonances. The best plot to examine for this purpose is the Dalitz plot (see Appendix A for a detailed explanation). Figure 22 shows the Dalitz plots of both reactions in terms of the pion kinetic energies in the center-of-mass system of the whole reaction. A concentration of the dots (each dot represents

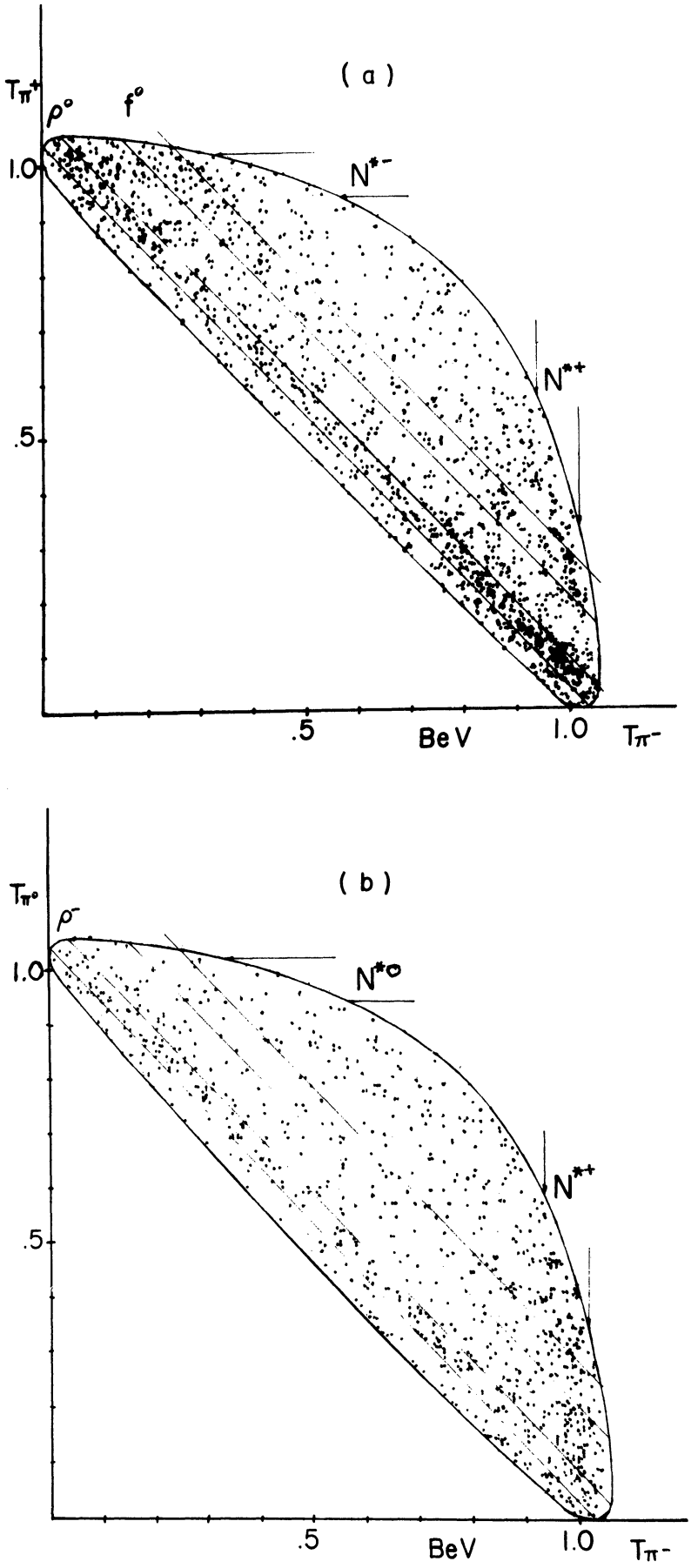

Figure 22. Dalitz plots for reactions (2) and (3).

one event) in a vertical or horizontal band indicates a resonance in the pion-nucleon system, since the pion-nucleon effective mass is expressed by

$$M^2_{(\pi,N)} = W_{TOT}^2 - M^2_{\pi 2} - 2W_{TOT}(M_{\pi 2}+T_{\pi 2})$$

where W_{TOT}, $M_{\pi 2}$ and $T_{\pi 2}$ are total center-of-mass energy, mass and kinetic energy of the second pion in the center of mass of the whole reaction. It is seen from the formula that $M^2(\pi,N)$ is a linear function of the kinetic energy of the other pion. The pion-pion resonances are recognized by the concentration along 135° lines, since the pion-pion mass is described by

$$M^2_{(\pi\pi)} = M_N^2 - W_{TOT} + 2W_{TOT}(T_{\pi 1}+T_{\pi 2}+M_{\pi 1}+M_{\pi 2})$$

where M_N is the mass of the nucleon. In Figure 22 there are obvious concentrations along the 135° lines which indicate ρ°, f°, and ρ^-. In Figure 22b, there is a slight indication of isobar (1238,3/2,3/2) in the $\pi^\circ p$ system which appears as a concentration in a vertical band at a π^- kinetic energy of about 1000 MeV. This means that in Figure 22a there should be also some observation of this isobar, since the branching ratio $N^*(\pi^+n)/N^*(\pi^\circ p)$ is 1/2, regardless of the production mechanism. However, this band is almost not visible because resonances in the pion-pion system dominate. Any concentration of dots in a horizontal direction apparently does not exist. The reason for this may be that the ratio for $N^*(3/2,3/2)$ production is 4:2:1:0 for the modes

$\pi^\circ p:\pi^+ n:\pi^- p:\pi^- n$ (see Appendix B for proof), assuming the production is due to the exchange of a ρ meson.

Since the Dalitz plot (Figure 22) shows that there is a slight but definite concentration of dots around $T_{\pi^-} = 1000$ MeV for reaction (2), an attempt was made to estimate the N* production. Figure 23b shows the distribution of π° kinetic energy for those events inside the $N^*(\pi^\circ p)$ ($920 < T_{\pi^-} < 1020$ MeV) region. The lower horizontal line shows the estimated background which was drawn by averaging the nonresonant area (neither N* nor ρ) in the Dalitz plot. The upper horizontal line shows the average value of N* events outside the ρ region. The events in between these two lines can be considered as due to N* production. We estimate that this amounts to about 90 events for reaction (2). By taking half of the amount we get for (2) we therefore estimate about 45 events for reaction (3). This corresponds to about a 0.35 mb cross section for all N^{*+} production via the reaction $\pi^- + p \rightarrow N^{*+} + \pi^-$.

5.5 STUDY OF f°-PEAK AND DETERMINATION OF f°-SPIN

The resonance around $M_{\pi\pi}$ of 1250 MeV has been also found by several other workers.[10-13] Since there is no such bump in reaction (2), this f° resonance is thought to be an isotopic singlet (T = 0) with even spin (L) (due to the generalized Pauli principle) provided isotopic spin is conserved in the reaction. The most probable quantum numbers originally assigned were T = 0, L = 2, parity +, G-parity +. However, recent work done by Frazer et al.,[16] indicates that the quantum numbers of f

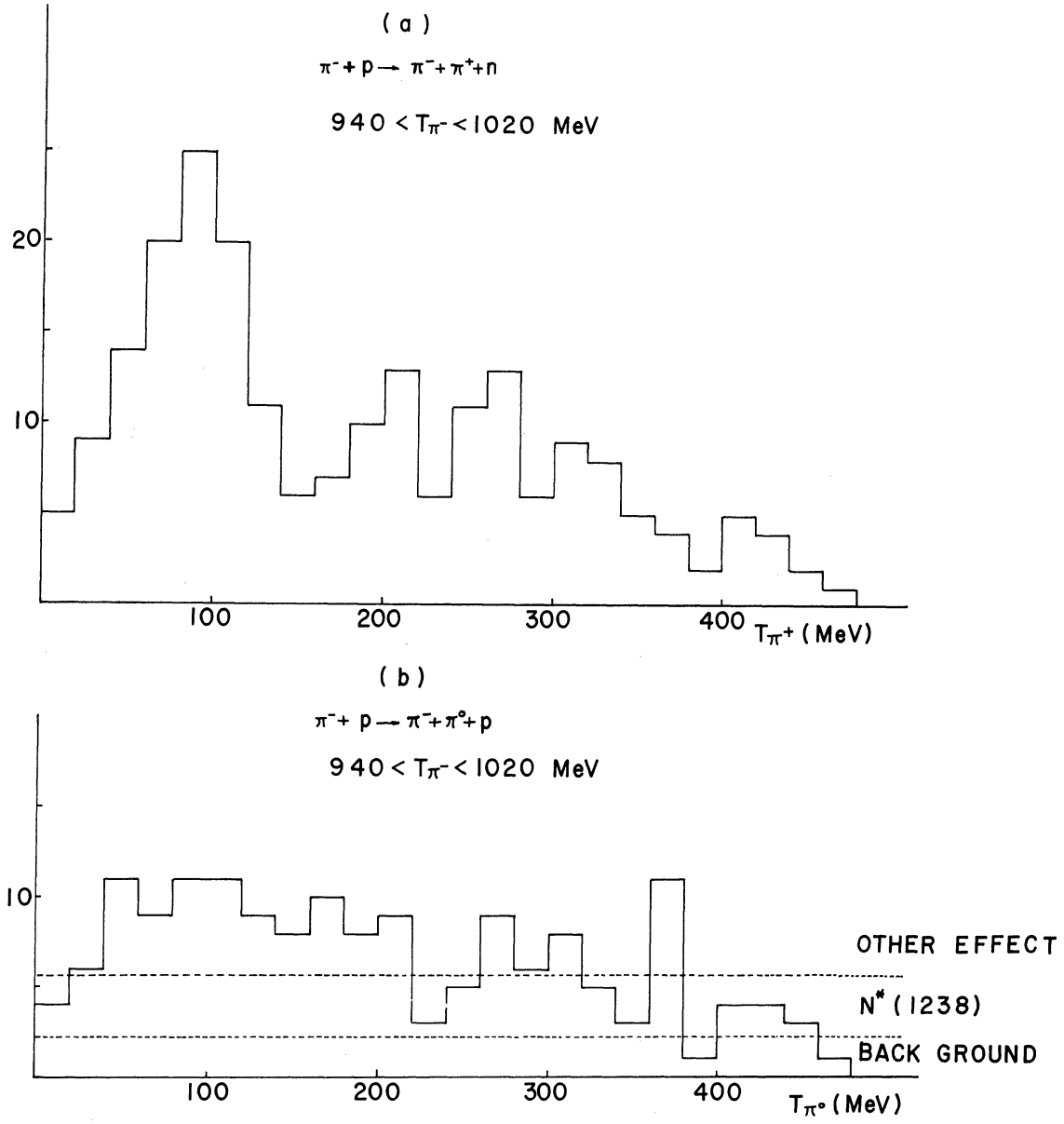

Figure 23. Distribution of π^+ and π° kinetic energy for events inside the N^{*+}-region.

may be T = 1, L = 1, and parity -, G-parity +. According to this viewpoint the recently discovered B-meson (ω-pion resonance[40]) would be the T_Z=+1 member of the f meson. In fact the angular distribution given in Refs. 12 and 37 gives a better fit to L = 1 than L = 2.

Because of the poorer statistics in this case, as compared to the ρ° case, it is difficult to make the same type of analysis. However, we can draw the following conclusions from the angular distribution of cos Θ (defined in the previous section for ρ). Figure 24 shows the distribution of cos Θ in the f region ($1170 < M_{\pi\pi} < 1330$ MeV) for Δ^2 of less than $20\mu^2$. Figure 24a shows reaction (3) while Figure 24b shows reaction (2). We see almost no asymmetry for reaction (3) and a heavy asymmetry for reaction (2), which is just the reverse of the phenomena we saw in the ρ case.

The shaded area in Figure 24 shows the random subtraction of N^{*+} events from the Dalitz plot taking a constant density along the vertical N^{*+} band. This amounts to 10 events from Figures 24a and 24c and 13 events from Figure 24b. This subtraction seems very reasonable, although the conclusions drawn below are not weakened appreciably if this subtraction is not made. It is certain, however, that the forward peak in the f° region (Figure 24a) is to a large extent caused by N* production.

The lack of asymmetry in the cos Θ distribution for f° is already good evidence against T = 1, L = 1 for f, since the T = 1, L = 1, ρ° from the same reaction shows a large asymmetry through the ρ° resonance.

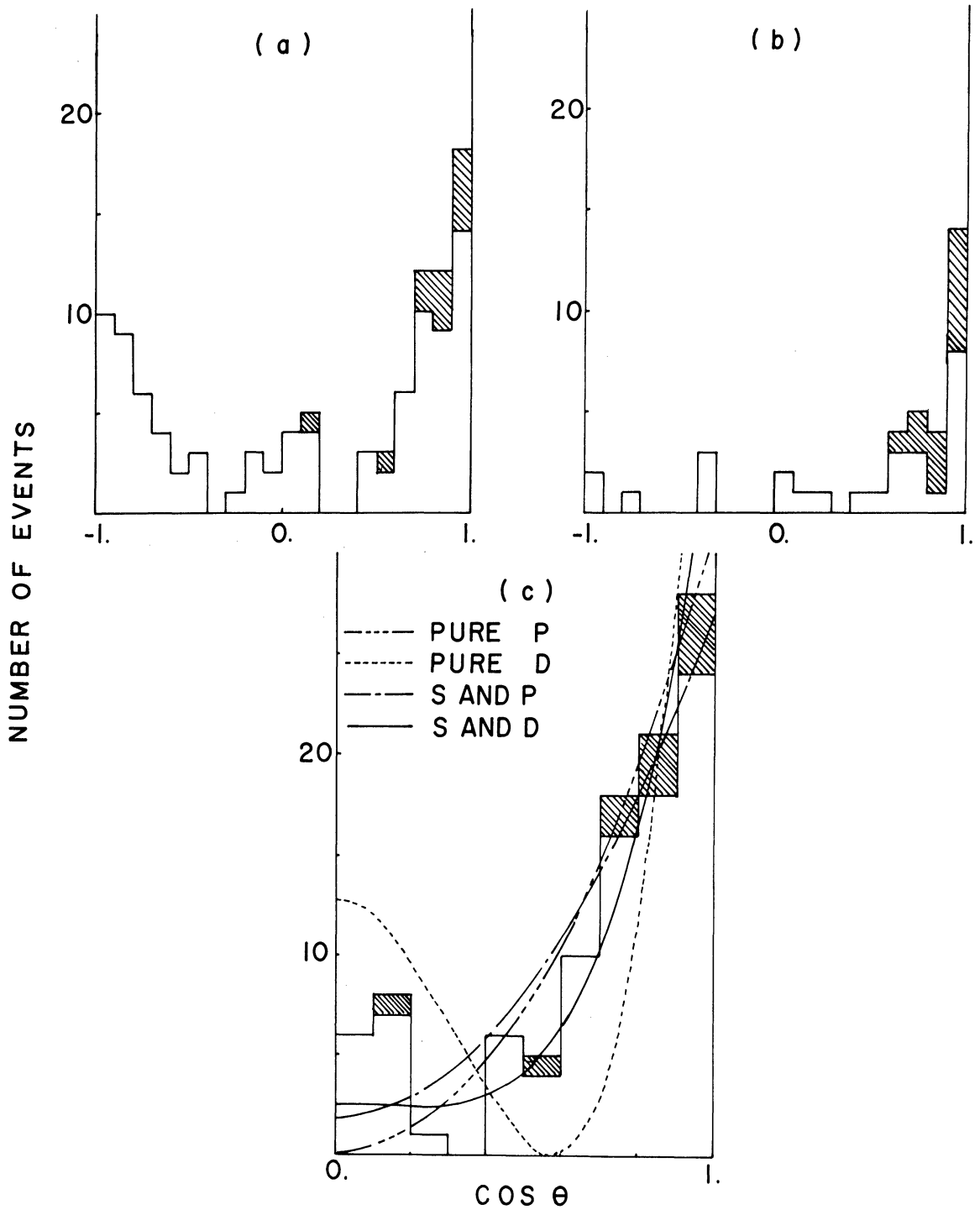

Figure 24. Distribution of cos Θ for events inside the f° mass.

We now attempt to determine the f°-spin from Figure 24a. Because of the symmetry of the f° angular distribution we have folded it about $\cos\theta = 0$ (Figure 24c). The normalized least squares fits to $A+B\cos\theta+C\cos^2\theta$ (s- and p-wave) and $A+B\cos^2\theta+C\cos^4\theta$ (s- and d-wave) are shown. Also shown as a comparison are $\cos^2\theta$ (pure p-wave) and $1-6\cos^2\theta+9\cos^4\theta$ (pure d-wave). The χ^2 probability for s- and d-wave is about 9% while for s- and p-wave it is less than 0.1%. The hump around $\cos\theta = 0$ and the steepness for large values of $\cos\theta$ is good evidence of the necessity of a $\cos^4\theta$ term, thereby ruling out L = 1 for f°. The hump around the center is not big enough to fit pure d-wave, but this is not surprising in view of the possible s-wave background and the interference between them. This gives good evidence against L = 1 (and, of course L = 0) for f°. We conclude that L = 2 is the most reasonable value for the f°-spin although we cannot rule out $L \geq 3$.

The Treiman-Yang angle test for f° (Figure 14c) for the one-pion exchange model does not give a result as good as that for ρ's. This might be caused by events preceding other than by one-pion exchange. If the reaction does not go through one-pion exchange, other processes can introduce any combination of f° polarization states which, therefore, can introduce any combination of Y_2^m terms ($m \neq 0$) into the angular distribution. This would allow practically any values for A, B, and C. This discrepancy in the Treiman-Yang angle does not weaken our conclusion against L = 1 since the angular distribution (Figure 24c) requires higher than second-order terms in $\cos\theta$.

An independent test was made for the consistency of the quantum numbers for the f particle on the basis of the di-pion mass spectrum (Figure 9). Assuming that f production occurs predominantly through one-pion exchange in the T = 1 and L = 1 channel, one would expect one-half as many events in an f^- peak as in the f°-peak. If one takes half of the events in the f°-peak above the phase space and subtracts them from the same mass region of Figure 9b, a definite dip occurs which falls far below the general appearance of the background. Moreover other processes, such as ω exchange, which can contribute to $\pi^-\pi^\circ p$ production and therefore possibly obscure any f^- peak, tend to make the ratio of total numbers of f° events to f^- events closer to unity; whereas the ratio we observe is at least 3 to 1, including background. The evidence, therefore, indicates that this ratio is not consistent with the T = 1, L = 1 assumption.

The lack of evidence for f^- formation also seems to rule out the possibility of T = 2 for f°, since pure T = 2 pion-pion scattering requires a 4.5 times <u>bigger</u> bump in f^- than f°. An experiment which is now in progress in this group (π^+ in deuterium) should give definite isotopic spin information on the f° as it will measure the ratio $(f^\circ \to \pi^\circ+\pi^\circ)/(f^\circ \to \pi^-+\pi^+)$. This ratio should be 1/2, 0 or 2 for T = 0, 1 or 2, respectively.

5.6 PARTIAL CROSS SECTIONS

We close this chapter by presenting cross sections for the different

types of reactions in this experiment. Below is a table showing the cross section of each reaction of interest. The total cross section for pion-proton interactions at our energy is fairly well known and the values we give are normalized to a total cross section 31.5 mb, obtained from the counter experiment by Diddens et al.[30] By doing this we do not have to take into account the kayon or muon contamination in the total path length scanned. In this table, the cross sections for neutrals (0 prongs) were obtained from another similar experiment[31] to fill an empty spot in our table.

TABLE VI

TYPES OF EVENTS AND CROSS SECTIONS
FOR 3.7 BeV/c π^-p INTERACTIONS

Type of Event	Cross Section (mb)
$\pi^- + p \rightarrow \pi^- + p$	4.74 ± 2.0
$\rightarrow \pi^- + p + \pi^\circ$	2.51 ± 0.5
$\rightarrow \pi^- + \pi^+ + n$	3.96 ± 0.7
→ other 2 prongs	8.32 ± 2.0
$\rightarrow \pi^- + \pi^- + \pi^+ + p$	1.71 ± 0.5
$\rightarrow \pi^- + \pi^- + \pi^+ + p\ \pi^\circ$	2.42 ± 0.7
$\rightarrow \pi^- + \pi^- + \pi^+ + \pi^+ + n$	1.00 ± 0.5
→ other 4 prongs	2.45 ± 0.7
→ 0 prongs	3.0 ± 1.0
$\rightarrow \geq 6$ prong and strange particles	1.04 ± 1.0
Total	31.5 mb

APPENDIX A

DALITZ PLOT AND LORENTZ INVARIANT PHASE SPACE

Consider the three body final state in center-of-mass system (e.g., $\pi^- + p \rightarrow \pi + \pi + N$) and define the variables

p_T total 4-momentum

M_i, T_i, p_i rest mass, kinetic energy and 4-momentum of ith particle

E_T, E_i energy of total and ith particle

M_{ij} effective mass of ith and jth particle

$\vec{p}_i$ 3-momentum of ith particle.

If there are no final state interactions or angular momentum preference the final state should be distributed in proportional to the energy density of final state

$$\rho \propto \int d^4p_1 d^4p_2 d^4p_3 \delta^4(p_1+p_2+p_3-p_T) \times \prod_{i=1}^{3} \delta(p_i^2+M_i^2) \quad . \tag{A-1}$$

The term $\delta(p_i^2+M_i^2)$ can be expressed in another form $\delta(E_i^2-E_i^{02})$, where $E_i^{02} = \vec{p}_i^{\,2}+M_i^2$. Therefore

$$\rho \propto \int d4p_1 d^4p_2 d^4p_3 \delta^4(p_1+p_2+p_3-p_T) \left[\prod_{i=1}^{3} \delta(E_i^2-E_i^{02}) \right]$$

$$\propto \int \frac{d^3p_1 d^3p_2 d^3p_3 \delta(p_1+p_2+p_3-p_T)}{E_1^{\,0} E_2^{\,0} E_3^{\,0}} \quad . \tag{A-2}$$

By carrying out the integration over d^3p_3

$$\rho \int \frac{d^3p_1 d^3p_2}{E_1^0 E_2^0 E_3^0} \delta(E) \qquad \text{(A-3)}$$

where $\delta(E)$ represents energy conservation. Now for further calculation we need information from 3-momentum conservation in the $\vec{p}_T = 0$ reference frame (Figure 25).

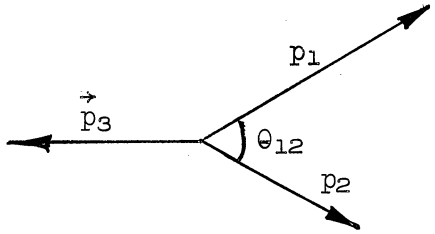

Figure 25. Momentum vector for 3-body final state in center-of-mass system.

$$\vec{p}_3^{\,2} = \vec{p}_1^{\,2} + \vec{p}_2^{\,2} - 2\vec{p}_1\vec{p}_2 \cos\theta_{12} \quad . \qquad \text{(A-4)}$$

Thus for given $|\vec{p}_1|$ and $|\vec{p}_2|$

$$2|\vec{p}_3||d\vec{p}_3| = 2|\vec{p}_1||\vec{p}_2|\,d(\cos\theta_{12}) \qquad \text{(A-5)}$$

and since

$$\vec{p}_i^{\,2} + M_i^2 = (M_i + T_i)^2,$$

$$|\vec{p}_i||d\vec{p}_i| = E_i dT_i \qquad \text{(A-6)}$$

then

$$\rho \propto \int \frac{|\vec{p}_1|^2 |p_2|^2}{E_1^0 E_2^0 E_2^0} |d\vec{p}_1||d\vec{p}_2| d\Omega_1 d\Omega_2 \delta(E)$$

$$= \int \frac{|\vec{p}_1||\vec{p}_2|}{E_3^0} d\Omega_1 d\Omega_2 dT_1 dT_2 \delta(E) \qquad \text{(A-7)}$$

where Ω_1, Ω_2 are the solid angles for particles 1 and 2. This integration over solid angle becomes a numerical factor times the integral over cos Θ_{12}

$$\rho \propto \int \frac{|\vec{p}_1||\vec{p}_2|}{E_3^0} dT_1 dT_2 d(\cos \Theta_{12}) \delta(E) \quad . \qquad \text{(A-8)}$$

The integration over dT_3 eliminates $\delta(E)$ and we get

$$\boxed{\rho \propto \int dT_1 dT_2} \quad . \qquad \text{(A-9)}$$

Therefore the differential of the density of final states is proportional to the area $dT_1 dT_2$ i.e., if we make a scattergram for T_1 and T_2, it should give a uniform distribution inside the kinematically allowed region.

The kinematically allowed region can be calculated by Eq. (A-4) and the energy equation

$$E_1 + E_2 + E_3 = E_T$$

by eliminating $\vec{p}_3$

$$2\vec{p}_1\vec{p}_2 \cos \Theta_{12} = E_T^2 + M_1^2 + M_2^2 + M_3^2 - 2E_T(E_1+E_2) + 2E_1E_2 \qquad \text{(A-10)}$$

The kinematically allowed region is the solution corresponding to $-1 \leq \cos \theta_{12} \leq +1$. We set $\cos \theta_{12} = 1$ and square the equation. Then two solutions of E_2 are obtained for each value of E_1. These two solutions give the kinematical limits.

Since we have the relation

$$\sqrt{M_{ij}^2+p_{ij}^2} + \sqrt{M_k^2+p_k^2} = E_T \qquad \text{(A-11)}$$

where $\vec{p}_{ij}$ is the 3-momentum of the ith and jth particle system. We express M_{ij}^2 by

$$M_{ij}^2 = (E_T-M_k)^2 - 2E_T T_k \quad . \qquad \text{(A-12)}$$

Therefore a Dalitz plot can be made in terms of M_{ij}^2. Since the density is uniform, the probability that the two-particle mass becomes M_{ij} is proportional to the length between the corresponding kinematically allowed limits. This probability is invariant under Lorentz transformations and we refer to it as "phase space" in graphs where we plot number of events versus M_{ij}.

APPENDIX B

PRODUCTION AND DECAY RATIO OF NUCLEON ISOBAR (1238,3/2,3/2)

Assume the reaction $\pi^- + p \rightarrow N^*_{\frac{3}{2}\frac{3}{2}} + \pi$ goes through ρ meson exchange (Figure 26).

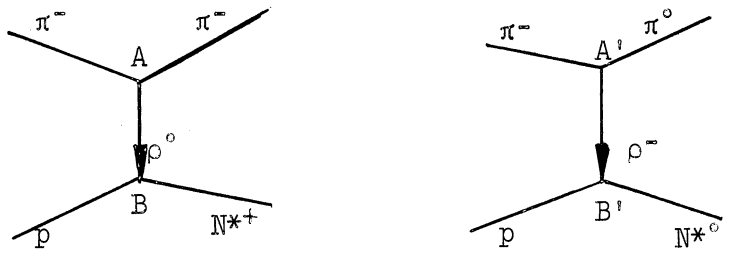

Figure 26. One-meson exchange diagram for N* production.

We use labels A and A' for the meson vertices and B and B' for the nucleon vertices (see Figure 26). On the vertices A and A'

$$\pi^- \rightarrow \pi^-(o) + \rho^o(-) \tag{B-1}$$

and for the isotopic spin functions we have

$$|\pi^-> \;=\; |1,-1> \rightarrow \frac{1}{\sqrt{2}} \left(\pi^o\rho^- - \pi^-\rho^o \right) \quad . \tag{B-2}$$

This relation shows that the probability of π^- going to both A and A' vertices is the same.

For the B and B' vertices the reaction is

$$p + \rho^o(-) \rightarrow N^{*+}(o) \tag{B-3}$$

so we construct

$$|\rho^- p> = \sqrt{\frac{1}{3}}\left|\frac{3}{2}, -\frac{1}{2}\right> + \sqrt{\frac{2}{3}}\left|\frac{1}{2}, -\frac{1}{2}\right> \qquad \text{(B-4a)}$$

$$|\rho^\circ p> = \sqrt{\frac{2}{3}}\left|\frac{3}{2}, \frac{1}{2}\right> - \sqrt{\frac{1}{3}}\left|\frac{1}{2}, \frac{1}{2}\right> \qquad \text{(B-4b)}$$

where the coefficients are Clebsh-Gordon coefficients for combining angular momentum.[35] Therefore we have a 2 to 1 ratio for production of isotopic spin 3/2 states from ρ°+p and ρ^-+p.

Now, the possible decay modes of N*'s are

$$N^{*+}\left|\frac{3}{2}, \frac{1}{2}\right> \rightarrow \pi^+ + n$$
$$\rightarrow \pi^\circ + p \qquad \text{(B-5a)}$$

$$N^{*\circ}\left|\frac{3}{2}, -\frac{1}{2}\right> \rightarrow \pi^\circ + n$$
$$\rightarrow \pi^- + p \qquad \text{(B-5b)}$$

and the isotopic spin functions for these modes can be written

$$\left|\frac{3}{2}, \frac{1}{2}\right> = \sqrt{\frac{2}{3}}\left|\pi^\circ p\right> + \sqrt{\frac{1}{3}}\left|\pi^+ n\right> \qquad \text{(B-6a)}$$

$$\left|\frac{3}{2}, -\frac{1}{2}\right> = \sqrt{\frac{1}{3}}\left|\pi^- p\right> + \sqrt{\frac{2}{3}}\left|\pi^\circ n\right> \quad . \qquad \text{(B-6b)}$$

They are independent of production mechanism. Since we cannot see the π°n decay mode, only 1/3 of the isotopic spin state $\left|\frac{3}{2}, -\frac{1}{2}\right>$ is observable. $N^{*+}\left|\frac{3}{2}, \frac{1}{2}\right>$ decays into either π^+n or π°p, and the ratio is 1 to 2. By combining (B-4) and (B-6), we get that the ratios $N^*(\pi^\circ p)$; $N^*(\pi^+ n)$, $N^*(\pi^- p)$ are 4:2:1.

For N^{*-} production by one-particle exchange, one must exchange a doubly charged particle. This is not possible for ρ meson exchange since the ρ meson has T = 1. Therefore, we get the ratio of the N*'s should be

$$N^*(\pi^\circ p); \quad N^*(\pi^+ n); \quad N^*(\pi^- p); \quad N^*(\pi^- n) \rightarrow 4:2:1:0$$

provided the production is due to pure ρ exchange.

APPENDIX C

ANGULAR DISTRIBUTION OF ρ^- DECAY ASSUMING ω° EXCHANGE

Consider the reaction

$$\pi^- + p \rightarrow \rho^- + p$$

which can exchange either a π° or ω° without violating any conservation law. Assume the quantum number of the ρ is $T = 1$ (1^{-+}). The following momentum diagram can be drawn in the rest system of the ρ (Figure 27).

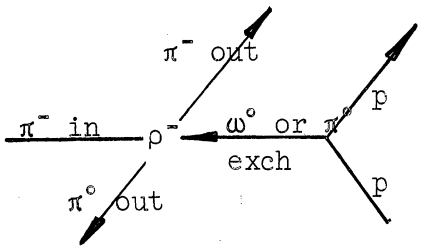

Figure 27. One-particle exchange diagram in rest system of final di-pion.

Since for π° exchange the angular distribution is well discussed previously in this report, we will only discuss the ω°-exchange mechanism.

Let ω_a^b represent the spin function of the ω exchange, where a and b are the spin and z-component of spin ($a = 1$ for the ω). Since we assume the parity in this reaction is conserved, the ω-π orbital angular momentum should be 1 (ρ, ω, π all have parity = -). Thus we can have the wave functions

$$\pi_{in} + \omega_{exch} \rightarrow \frac{1}{\sqrt{2}} (Y_1^1\omega_1^\circ - Y_1^\circ\omega_1^1) = \rho_1^1$$

$$\rightarrow \frac{1}{\sqrt{2}} (Y_1^{-1}\omega_1^\circ - Y_1^\circ\omega_1^{-1}) = \rho_1^{-1}$$

$$\rightarrow \frac{1}{\sqrt{2}} (Y_1^{-1}\omega_1^1 - Y_1^1\omega_1^{-1}) = \rho_1^\circ$$

where Y's are spherical harmonics, and ρ_1^m are the ρ spin functions.

Now if we take the axis of incoming π and exchange ω as z-axis, the z-component of orbital angular momentum has to be 0. Therefore only Y_1° terms are allowed and we get some general combination of ρ_1^{-1} and ρ_1^{-1} for the ρ-spin function. Thus the Y's for the final state pions arise as

$$Y_1^\circ(A\omega_1^1 + B\omega_1^{-1}) = A\rho_1^1 + B\rho_1^{-1} \rightarrow AY_1^1 + BY_1^{-1} \quad .$$

Parity is conserved on the nucleon vertex so the whole process is independent of the polarity of exchange particles. Therefore coefficient $|A| = |B|$, thus we get for the density of final state π^-

$$I(\pi^-) = |AY_1^1 + BY_1^{-1}|^2 \propto \sin^2\theta \left| e^{i(\phi+\delta)} \pm e^{-i\phi} \right|^2$$

where δ is the phase angle between A and B. If we experimentally integrate over ϕ by not observing the ϕ angle, we get

$$I(\pi^-) \propto \sin^2\theta \quad .$$

REFERENCES

1. M. Roos, Rev. Mod. Phys., 35, 374 (1963).

2. A. Rosenfeld, Tables of Elementary Particles (private publication 1963).

3. Y. Y. Lee, W.D.C. Moebs, B. P. Roe, D. Sinclair, and J. C. Vander Velde, Bull. Am. Phys. Soc. 8, 325 (1963).

4. J. C. Vander Velde, D. Sinclair, B. P. Roe, W.D.C. Moebs, and Y. Y. Lee, Bull. Am. Phys. Soc. 8, 325 (1963).

5. Y. Y. Lee, W.D.C. Moebs, B. P. Roe, D. Sinclair, and J. C. Vander Velde, Phys. Rev. Letters 11, 508 (1963).

6. W. R. Frazer and J. R. Fulco, Phys. Rev. 117, 1609 (1960).

7. A. R. Erwin, R. March, W. D. Walker, and E. West, Phys. Rev. Letters 6, 628 (1961).

8. D. Camoney, UCRL 9886 (1961).

9. E. Pickup, D. K. Robinson, and E. O. Salant, Phys. Rev. Letters 7, 192 (1961).

10. W. Selove, V. Hagopian, H. Brody, A. Baker, and E. Leboy, Phys. Rev. Letters 9, 272 (1962).

11. J. J. Veillet, J. Hennessy, H. Bingham, M. Bloch, D. Drijard, A. Lagarrigue, P. Mittner, A. Rousset, G. Bellini, M. di Corato, E. Fiorini, and P. Negri, Phys. Rev. Letters 10, 29 (1963).

12. Z.G.T. Guiragossian, UCRL 10731, (1963).

13. D. M. Ritson, Techniques of High Energy Physics, p. 108, (Interscience publishers, 1961).

14. T. Regge, Nuovo Cimento 14, 951 (1959), and 18, 947 (1960).

15. G. F. Chew and S. C. Frautschi, Phys. Rev. 126, 1202 (1962).

16. W. R. Frazer, S. H. Patil, N. Xuong, Phys. Rev. Letters 12, 178 (1964).

REFERENCES (Continued)

17. G. F. Chew and F. E. Low, Phys. Rev. 113, 1640 (1959).

18. V. Hagopian and W. Selove, Phys. Rev. Letters 10, 533 (1963).

19. E. Hart, BNL-BCG Internal Report J-22 (1962).

20. R. Raw, BNL-BCG Internal Report J-18 (1961).

21. W. J. Fickinger, J. Sandweiss, J. R. Sanford, The Cosmotron Parallel Plate Velocity Spectrometer (Cosmotron internal report 1961).

22. J. R. Sanford, The Separated Beam to the 20 in. Bubble Chamber at the AGS (BNL internal report 1962).

23. V. T. Cocconi, T. Fazzini, G. Fidecaro, M. Legros, N. H. Lipman, and A. W. Merrison, Phys. Rev. Letters 5, 19 (1960).

24. W. F. Baker, R. L. Cool, E. W. Jenkins, T. F. Kycia, S. S. Lindenbaum, W. A. Love, D. Lüers, J. A. Niederer, S. Ozaki, A. L. Read, J. J. Russell, and C. L. Yuan, Phys. Rev. Letters 7, 101 (1961).

25. G. F. Chew, M. Gell-Mann, and A. H. Rosenfeld, Scientific American 210, 74 (1964).

26. J. C. Vander Velde, Univ. of Mich. Bubble Chamber Group Research Note HI-1 and HI-3 (1963).

27. A. H. Rosenfeld and J. C. Snyder, UCRL 9098 (1960).

28. J. Berge, F. Solmitz and H. Taft, Rev. of Sci. Instr. 32, 538 (1961).

29. J. Orear, UCRL 8417 .

30. A. Diddens, E. Jenkins, T. Kycia and K. Riley, Phys. Rev. Letters 10, 262 (1962).

31. V. Hagopian, The reaction $\pi^- + p \rightarrow \pi^- + \pi^+ +$ nculeon at 3 BeV/c (Univ. of Penn, Dissertation 1963).

32. S. B. Treiman and C. N. Yang, Phys. Rev. Letters 8, 140 (1962).

REFERENCES (Concluded)

33. P. Eberhard and M. Pripstein, A possible explanation of the observed asymmetry in ρ° decay (preprint 1963).

34. W. J. Fickinger, D. K. Robinson, E. O. Salant, Phys. Rev. Letters 10, 457 (1963).

35. E. U. Condon and G. H. Shortly, Theory of Atomic Spectra, p. 76, (Cambridge University Press, 1957).

36. F. Selleri, Phys. Letters 3, 76 (1962).

37. L. Bondar, K. Bongartz, M. Deutschmann, H. Weber, D. C. Colley, W. P. Dodd, J. Simmons, B. Tallini, J. Moebes, B. Nellen, G. Winter, E. Lohrmann, E. Ranbold, G. Wolf, J. M. Brownlee, I. Butterworth, F. I. Campayne, M. Ilibotson, Y. S. Liu, N. N. Biswas, I. Derado, D. Lüers, G. Lütjens, M. Schmitzi, Phys. Letters 5, 153 (1963).

38. G. Breit and P. Wigner, Phys. Rev. 49, 519 (1936).

39. Y. Y. Lee, B. P. Roe, D. Sinclair and J. C. Vander Velde, An Experimental Study of the ρ-Meson as π-π Scattering Resonance (to be published, 1964).

40. A. Maris, R. L. Lander, W.A.W. Mehlhop, N. Xuong and P. M. Yager, Phys. Rev. Letters 11, 381 (1963).

41. J. M. Blatt and V. F. Weisskopf, The Theoretical Nuclear Physics, p. 406 (John Wiley and Sons, 1952).